Insights into the palaeobiology of an early Homo infant: multidisciplinary investigation of the GAR IVE hemi-mandible, Melka Kunture, Ethiopia

Adeline Le Cabec, Thomas Colard, Damien Charabidze, Catherine Chaussain, Gabriele Di Carlo, Sabine Gaudzinski-Windheuser, Jean-Jacques Hublin, Rita T Melis, Laura Pioli, Fernando Ramirez-Rozzi, et al.

scientific reports

Check for updates

OPEN

Insights into the palaeobiology of an early *Homo* infant: multidisciplinary investigation of the GAR IVE hemi-mandible, Melka Kunture, Ethiopia

Adeline Le Cabec[1,2]✉, Thomas Colard[3], Damien Charabidze[4], Catherine Chaussain[5], Gabriele Di Carlo[6], Sabine Gaudzinski-Windheuser[7], Jean-Jacques Hublin[1], Rita T. Melis[8,9], Laura Pioli[9], Fernando Ramirez-Rozzi[5,10] & Margherita Mussi[8,11]✉

Childhood is an ontogenetic stage unique to the modern human life history pattern. It enables the still dependent infants to achieve an extended rapid brain growth, slow somatic maturation, while benefitting from provisioning, transitional feeding, and protection from other group members. This tipping point in the evolution of human ontogeny likely emerged from early *Homo*. The GAR IVE hemi-mandible (1.8 Ma, Melka Kunture, Ethiopia) represents one of the rarely preserved early *Homo* infants (~ 3 years at death), recovered in a richly documented Oldowan archaeological context. Yet, based on the sole external inspection of its teeth, GAR IVE was diagnosed with a rare genetic disease–amelogenesis imperfecta (AI)–altering enamel. Since it may have impacted the child's survival, this diagnosis deserves deeper examination. Here, we reassess and refute this diagnosis and all associated interpretations, using an unprecedented multidisciplinary approach combining an in-depth analysis of GAR IVE (synchrotron imaging) and associated fauna. Some of the traits previously considered as diagnostic of AI can be better explained by normal growth or taphonomy, which calls for caution when diagnosing pathologies on fossils. We compare GAR IVE's dental development to other fossil hominins, and discuss the implications for the emergence of childhood in early *Homo*.

The pattern and timing of modern human life history is unique in involving an extended period of growth[1]. This provides more time not only for somatic development and protracted brain growth[2,3], but also to learn survival skills[4]. The offspring is thus dependent upon more parental care over a longer time, and sexual maturity is postponed[5]. In modern humans, life history stages successively involve infancy, childhood, a juvenile phase, adolescence, and finally adulthood. Different kinds of feeding strategies and dental development stages characterize these phases. Following these criteria, infancy can be subdivided into two stages. First, the "nursing phase" takes place from birth to 6 months, when the infant exclusively relies on breastfeeding and starts erupting its

[1]Department of Human Evolution, Max Planck Institute for Evolutionary Anthropology, Deutscher Platz 6, 04103 Leipzig, Germany. [2]Univ. Bordeaux, CNRS, MCC, PACEA, UMR 5199, 33600 Pessac, France. [3]Department of Orthodontics, University of Lille, Lille University Hospital, 59000 Lille, France. [4]UMR 8025, Centre d'Histoire Judiciaire, University of Lille, 59000 Lille, France. [5]UR 2496 Orofacial Pathologies, Imaging and Biotherapies. Dental School Université de Paris, AP-HP- Hôpital Bretonneau - Service Odontologie CRMR Métabolisme du Phosphore et du Calcium (OSCAR, ERN Bond), Paris, France. [6]Department of Oral and Maxillofacial Sciences, Unit of Pediatric Dentistry, Sapienza University of Rome, Rome, Italy. [7]MONREPOS Archaeological Research Centre and Museum for Human Behavioural Evolution, Römisch-Germanisches Zentralmuseum, Leibniz-Forschungsinstitut Für Archäologie and Institute of Ancient Studies, Johannes Gutenberg–University Mainz, Schloss Monrepos, 56567 Neuwied, Germany. [8]Italian Archaeological Mission at Melka Kunture and Balchit, Rome, Italy. [9]Dipartimento Di Scienze Chimiche E Geologiche, Università Degli Studi Di Cagliari, Cittadella Universitaria, 09042 Monserrato (CA), Italy. [10]UMR 7206 CNRS MNHN UP Ecoanthropologie Musée de l'Homme, Paris, France. [11]Dipartimento di Scienze dell'Antichità, Università di Roma La Sapienza, Piazzale A. Moro 5, 00185 Rome, Italy. ✉email: adeline_lecabec@eva.mpg.de; margherita.mussi@fondazione.uniroma1.it

anterior deciduous teeth. Second, the "suckling phase" spans from 6 months to 3 years and involves supplementing complementary food to supply the nutrients not sufficiently present in quantity or quality in the mother milk to enable the fast postnatal brain growth, and the eruption of all deciduous teeth. Weaning is one of the pivotal life history traits occurring during ontogeny: this is a long process involving a transition from exclusive breastfeeding to the progressive introduction of solid food, towards total cessation of mother milk consumption (fully weaned infants) and full reliance on solid diet[6,7], and eventually feeding self-sufficiency. During hominin evolution, major changes in weaning and feeding behaviour may have occurred with early *Homo*, especially involving the reduction in dental size and dietary shifts to focus on food items more energy dense and easier to masticate, and on an increase in meat and fat consumption and food sharing[3,8,9]. Known as the "Expensive-Tissue Hypothesis"[8], this energy-rich diet would have enabled meeting the requirements of this demanding postnatal brain growth and achieving adult brain size by the end of childhood in humans. Following infancy, "childhood" spreads from 3 to 6 years of age when modern human weaned infants show all of their deciduous teeth in functional occlusion, although they cannot yet fully process an adult diet, due to their relatively small size and thin enamel[5]. In modern humans, the end of childhood is marked by the eruption of the permanent first molar (M1) at ~ 6 years of age[1], and the attainment of adult brain size[10].

In this context, fossil teeth are especially valuable not only because their recovery enables comparing developmental stages between fossil hominins and modern humans but also because dental hard tissues record their own growth and maturation as well as stressful events experienced by the organism[11]. In the tooth microstructure, stress events may manifest as accentuated lines and remain non-specific[12–14]. A specific accentuated growth marking called the neonatal line is often identifiable in the enamel and dentine of the deciduous teeth and in the mesial cusps of the permanent first molar which start mineralizing in utero[15,16].

During both infancy and childhood, protection and food provisioning by adults of the group (parents or others) is crucial for the child's survival. Understanding the modality and time of emergence of this unique modern life history pattern is currently one of the most debated topics in human evolution[9,17,18].

GAR IVE (full name: MK 81 GAR IVE 0043) is a fragmentary right hemimandible with a partial mixed dentition, recovered in layer E at the Garba IV site of the Melka Kunture complex (Upper Awash, Ethiopia) (Fig. 1). This fossil was attributed to *Homo erectus* s.l.[19], and its age at death was estimated to be 2–3.5 years[20,21]. With the recent discovery of *H. erectus* s.l. remains in association with Acheulean and Oldowan artifacts at Gona (Afar, Ethiopia)[22], GAR IVE is one of the rare early *Homo* remains recovered from the beginning of the Early Pleistocene, in the context of proper archaeological excavations providing contextual information on hominin activities[23]. GAR IVE was found with Oldowan industry and faunal remains in layer E, later dated to ~1.8 Ma (Fig. 1b–d)[24–28]. The deposits of Garba IV were dated and arranged in sequence in a thoroughly established chronostratigraphy[26,29], which was evaluated again during fieldwork in 2013 and 2017.

Previous studies reported GAR IVE as being affected by a rare genetic disease *amelogenesis imperfecta* (AI)[19], although they were only based on classical radiographs and SEM imaging of epoxy replicas of the tooth surface[19,30]. Zanolli and colleagues worked on CT data, but did not re-evaluate this diagnosis[21]. Amelogenesis imperfecta encompasses a group of developmental conditions[31] altering the enamel structure and making teeth fragile[32]. The main diagnostic criteria may involve a marked reduction in enamel thickness frequently concerning both deciduous and permanent teeth, enamel pits or linear hypoplasia not associated with any noticeable developmental defects in the other dental tissues, a brown colouration of the enamel, or taurodontism (enlargement of the pulp cavity associated with a lowering of the roof of the pulp chamber and root furcation level, giving the impression of a partial to complete fusion of the tooth roots)[31–36]. In some AI variants, enamel defects may be associated with other types of syndromes occurring in other parts of the human body (e.g., kidney diseases)[32,37,38]. In clinics, a differential diagnosis requires the knowledge of medical and family history of the patients, of their genetic profile, as well as of their conditions of development and life. Thus, AI patients mostly suffer from early tooth loss, severe embarrassment, eating difficulties and pain, requiring early and complex restorative treatments[38].

Genetic diseases are of particular interest as they happen to be transmitted along a lineage affecting multiple generations, and they may occur with variable frequencies, in the case of AI, ranging from 1:700 to 1:14 000[38]. According to Zilberman et al.[19,30], the presence of AI in GAR IVE would provide evidence of genetic continuity from early *Homo* to modern humans. Yet, this claim has to be considered with caution since the molecular mechanisms causing this pathology are complex and may involve several genes and combinations of genes[39]. Such a genetic continuity is unlikely to be so straightforward. Furthermore, Trinkaus[40] has suggested that any variant of this pathology would have involved the need for enhanced maternal care to supply the young child with sufficient nutrients and permit its survival to some extent[40].

Given the putative consequences of this disease on the specimen's morphology and the potential implications of living with AI during the Pleistocene, we aim to reassess the diagnosis of AI by analyzing tooth surface features and by exploring the fine internal structure of the bone and teeth using synchrotron imaging. We compare the GAR IVE teeth with teeth from modern human patients, some with documented forms of AI. Because taphonomic processes may affect the preservation of the specimens and the features related to the AI diagnosis, our study includes the analysis of the associated faunal remains and the geological context in which GAR IVE was recovered in order to establish if particular features are due to taphonomy or to developmental alterations induced by the AI. In spite of the taphonomic damages undergone by the dental tissues, we provide some novel fragmentary yet still valuable palaeobiological data on the dental development of this early *Homo* infant.

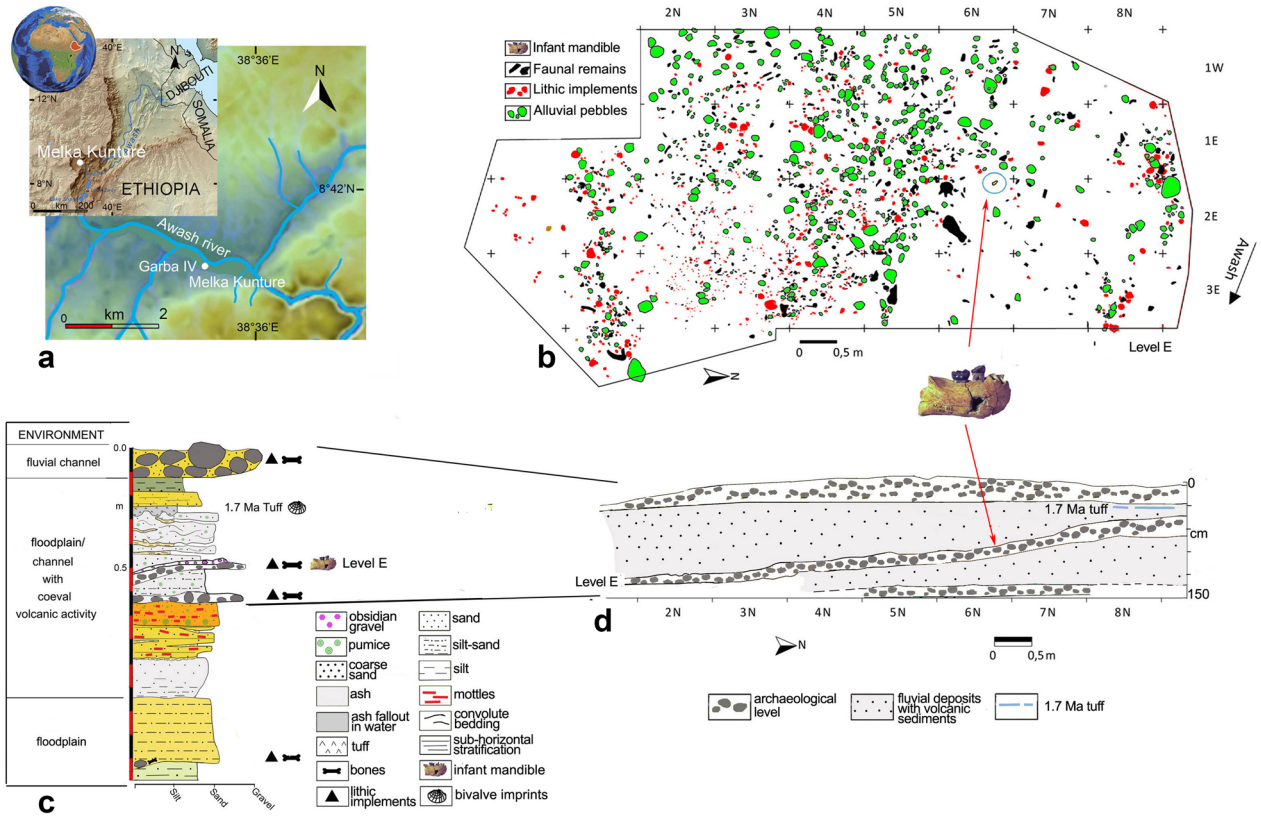

Figure 1. Garba IV site. (**a**) Location map of Melka Kunture and the Garba IV site (modified after https://upload.wikimedia.org/wikipedia/commons/2/24/Africa_satellite.jpg, https://commons.wikimedia.org/wiki/File:Awashrivermap.png, and https://data.humdata.org/dataset/ethiopia-elevation-model using QGIS software; https://qgis.org); (**b**) Plan of archaeological level E with position of GAR IVE (modified after Fig. 4A from Ref.[27]); (**c**) Stratigraphic log of Garba IV (Photoshop CS3; https://www.adobe-photoshop); (**d**) schematic cross-section of the archaeological levels (modified after Fig. 3B from Ref.[27]). The map of the Awash River (https://commons.wikimedia.org/wiki/File:Awashrivermap.png) is licensed under the Creative Commons Attribution-ShareAlike 3.0 license. The license terms can be found on the following link: http://creativecommons.org/licenses/by-sa/3.0/.

Results

After a brief description of the GAR IVE specimen, and especially of its dental development, we have compared the enamel features described as diagnostic of AI on GAR IVE to the enamel condition in teeth of modern-day AI patients. Then, we have explored the fine microstructure of the teeth and bone in light of taphonomic processes, recovered from the study of associated faunal remains, and the palaeoenvironmental reconstruction of the fossilisation context of GAR IVE.

Description of GAR IVE. The GAR IVE right hemimandible (Fig. 2) preserves both erupted deciduous molars ($LRdm_1$ and $LRdm_2$). The $LRdm_1$ is considerably worn (yet preserving a complete rim of enamel) and super-erupted above the occlusal level. The germ of the permanent first molar (LRM_1) is partially exposed at the posterior part of the specimen, as the mandibular ramus is missing. Its crown does not present any abnormal morphological features; to note that its occlusal surface shows extensive wrinkling, yet this LRM_1 looks similar to that of other fossil hominins (Fig. 3). The anterior portion of GAR IVE shows a greenstick fracture on its lingual side, suggesting this occurred peri-mortem, when the bone would have retained a certain level of collagen and moisture, thus still be fresh and elastic to some extent[41]. This fracture leaves the permanent lateral incisor (LRI_2) visible and partially unprotected by its bony crypt. The germs of the permanent canine (LRC_1), third and fourth premolars (LRP_3 and LRP_4) are unerupted and protected inside the mandibular bone. The bone and teeth present various kinds of surface alterations.

Insights into GAR IVE's dental development. The synchrotron µCT scans show a loss of contrast between bone, enamel and dentine, the enamel-dentine junction being barely visible in some places (Fig. 4). Any estimation of age at death based on dental growth increments and virtual histology techniques is thus precluded. At best, the maturation stage of the permanent tooth germs may provide insights into GAR IVE's dental development (See Supplementary Text S1 for details). Following modern human standards[42], the overall calcification stages in GAR IVE would correspond to 4.5 years of age (with individual scores per tooth going up to 7.5 years for the P_3; see Supplementary Table S1). Using Kuykendall's regression equation[43], GAR IVE would

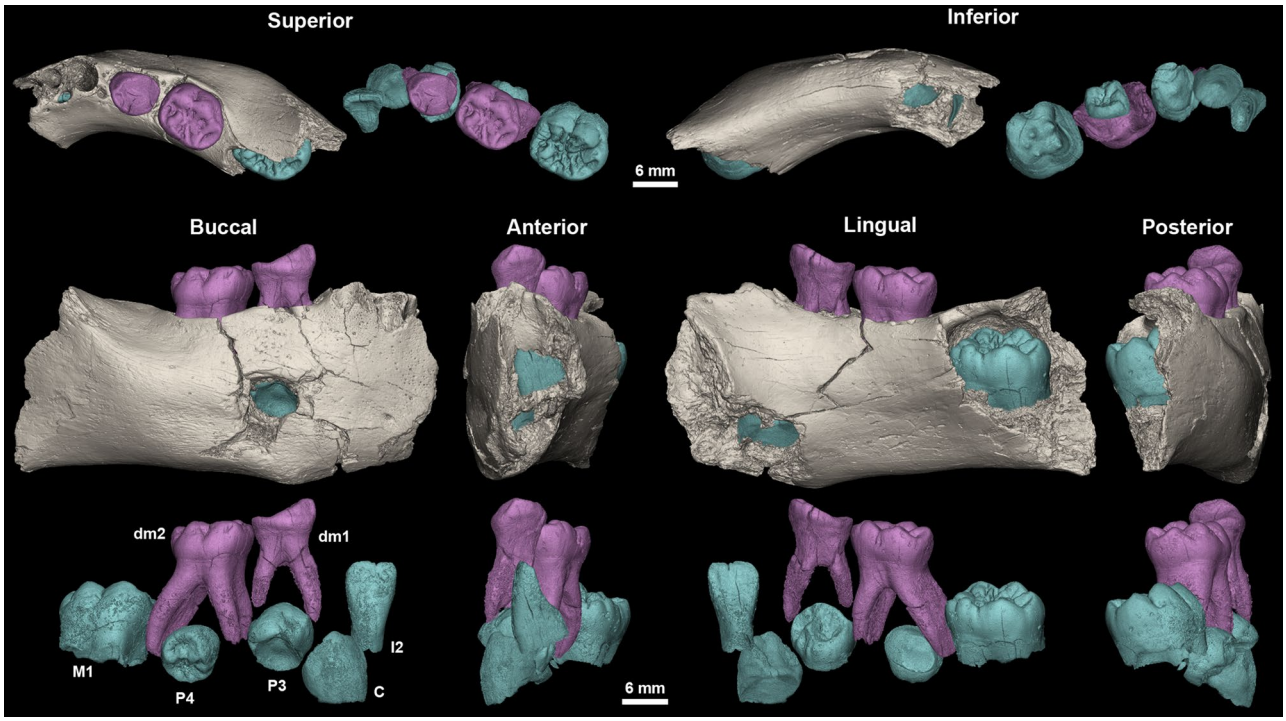

Figure 2. 3D models of the GAR IVE right hemi-mandible showing the mandibular bone (beige), the preserved deciduous molars (dm1 and dm2; pink) and the germs of the permanent teeth (I2: lateral incisor, C: canine, P3 and P4: first and second premolar, M1: first molar; blue). Superior, inferior, buccal, anterior, lingual and posterior views.

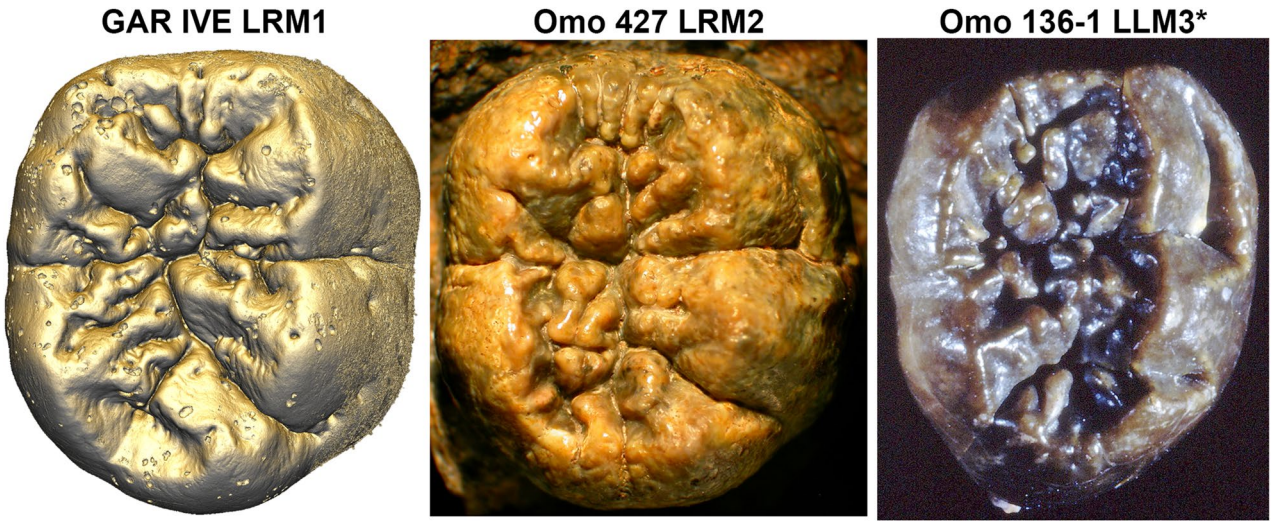

Figure 3. The occlusal surface of the LRM1 of GAR IVE (3D model) shows an amount of wrinkling comparable with that of other Plio-Pleistocene hominin molars such as the LRM2 of Omo 427 and the LLM3 of Omo 136-1 (*: flipped for illustrative purpose; both teeth were macro-photographed).

be 3.13 [2.14–4.12] years in a chimpanzee-equivalent model. Several fossil hominins died at developmental stages similar to that of GAR IVE, although any comparison highlights some modularity in the relative advancement of each tooth type across taxa (See Supplementary Text S1). In terms of calcification stages, KNM-ER 812 (*Paranthropus boisei*) seems to be developmentally the closest to GAR IVE and has an estimated age at death of 2.5–3.0 years. KNM-ER 1820 (*P. boisei*) is slightly more advanced than GAR IVE for an age at death similar to KNM-ER 812 (2.5–3.1 years). Overall, the calcification of the GAR IVE permanent tooth germs is less advanced than that of Sts 24 (*Australopithecus africanus*).

In spite of the taphonomic alteration of the dental tissues in GAR IVE, the synchrotron data revealed several accentuated lines in the LRP4 (Supplementary Text S1, Supplementary Fig. S13). These accentuated markings may correspond to multiple stressful events. However, it remains impossible to ascertain their cause which may

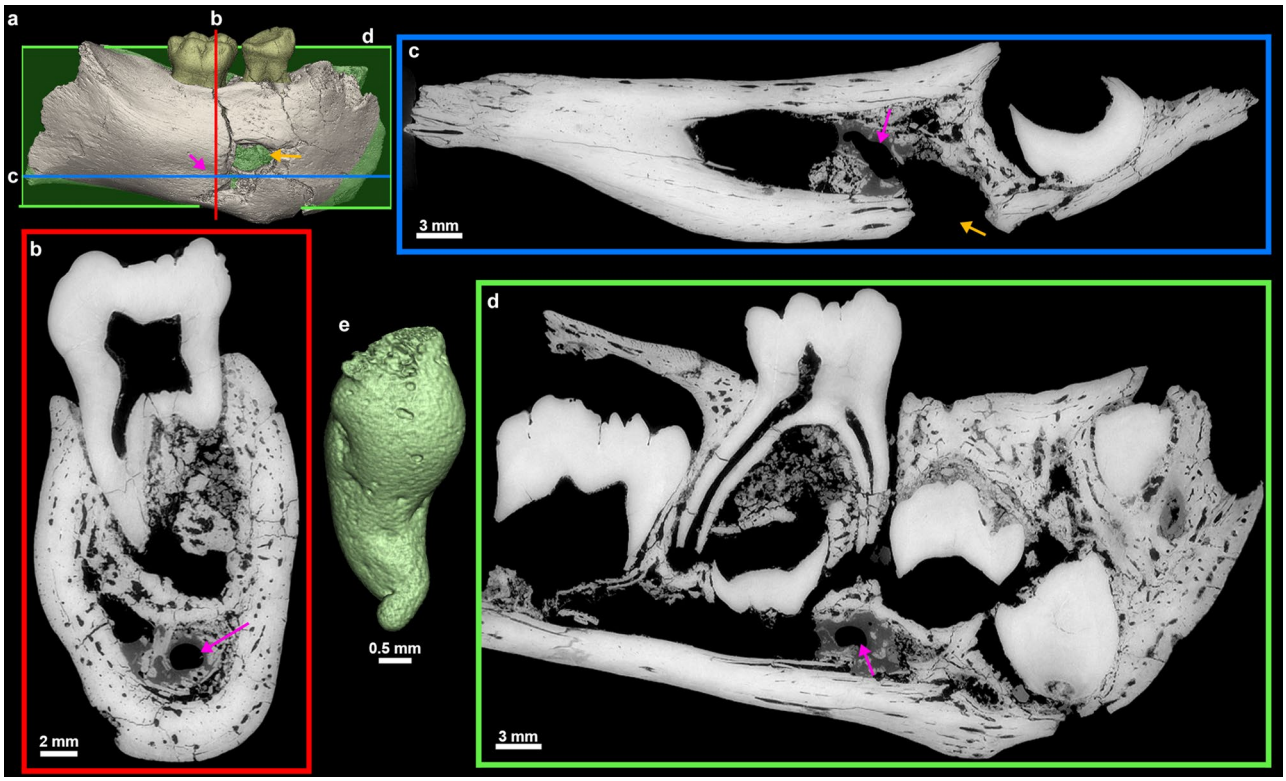

Figure 4. 3D model of the GAR IVE specimen (**a**), and frontal (**b**, red), axial (**c**, blue) and sagittal (**d**, green) planes of section to illustrate the morphology of the hole (orange arrow) located in the area of the mental foramen. Its inner negative imprint shows a complex shape which is little compatible with the shape of a carnivore tooth (**c**). To note an additional convoluted shape represented in green in 3D (pink arrow).

result from non-specific stress events in the life of the child. It also remains unknown whether these accentuated markings may witness disruptions in the growth process of GAR IVE, or even in its health. Assuming the initiation time of P4 (~ 2 years) and that the EDJ crest where the virtual slice was recorded formed ~ 3 months after the dentine horn tip, these were added to the times of formation of each stress line will yield an age of formation (Supplementary Text S1, Supplementary Table S9). Rough estimates following Dean et al.[44] show that they occurred every ~ 1.4 months, from 2.5 to 2.9 years of age (see Supplementary Text S1 for details). When superimposed with the lingual cusp of the GAR IVE LRP4, the most developed cusp of the DNH 35 (South African *Homo*) LRP4 matches with the purple stress "S3" in GAR IVE (see Supplementary Text S1 and Supplementary Fig. S14), which, following the DNH 35 growth pattern[45], would have then occurred at ~ the 796th day of life of GAR IVE (i.e., 2.18 years). Death occurred ~ 77 days later in GAR IVE, which correspond to ~ 873 days or ~ 2.4 years in the DNH 35 growth pattern. "S3" shows that the calculated estimation is slightly ahead of the developmental stage observed in other early *Homo* specimens (here by 6.5 months at most), yet this is may be accounted for by the variability which is not captured here, and by the uncertainties related to our measurements (e.g., the virtual section does not pass through the dentine horn tip).

Comparison of GAR IVE with teeth from modern-day AI patients. Among the three clinical cases of molars affected by AI, two have maximal enamel thickness values considerably smaller (0.3 mm and 0.6 mm, respectively; Fig. 5b and d.) than that of GAR IVE (2.2 mm; Fig. 5a). The third comparative sample has retained negligible portions of thick enamel in the cervical region (2.05 mm; Fig. 5c). Beyond being remarkably thin, the enamel of this tooth (Fig. 5c) is also considerable brittle and has been fractured during its time in occlusion. The enamel surface of the deciduous molar in Fig. 5b shows extensive and shallow pitting. Both deciduous molars (Fig. 5b and c) have underwent some restoration treatment in their occlusal basin. Overall, this contrasts with the enamel of GAR IVE which is exempt of any fracture or chipping (Figs. 4, 5a and Supplementary Fig. S19).

A taphonomic perspective to study a human remain. The largest bone loss on the buccal aspect of this right mandibular fragment is a hole which coincides with the anatomical position of the mental foramen (Figs. 2, 4). This cavity measures 5.5 mm in depth, 8.02 mm in outer width, from 3.4 to 4.1 mm in inner width and has a 7.51 mm-long tail on the outer bone surface. However, the fossil had been broken at the time of discovery, and curatorial activity led to some misalignment affecting the outline of this feature. Twenty-two faunal specimens of the Layer E also show evidence of perforations and characteristic damages (i.e., ~ 10% of the identified specimens) (Fig. 6, Supplementary Text S2; Supplementary Tables S10 and S11). Accordingly, the same agent was probably at work on fauna and hominin remains. We explored the impact of dermestid beetles

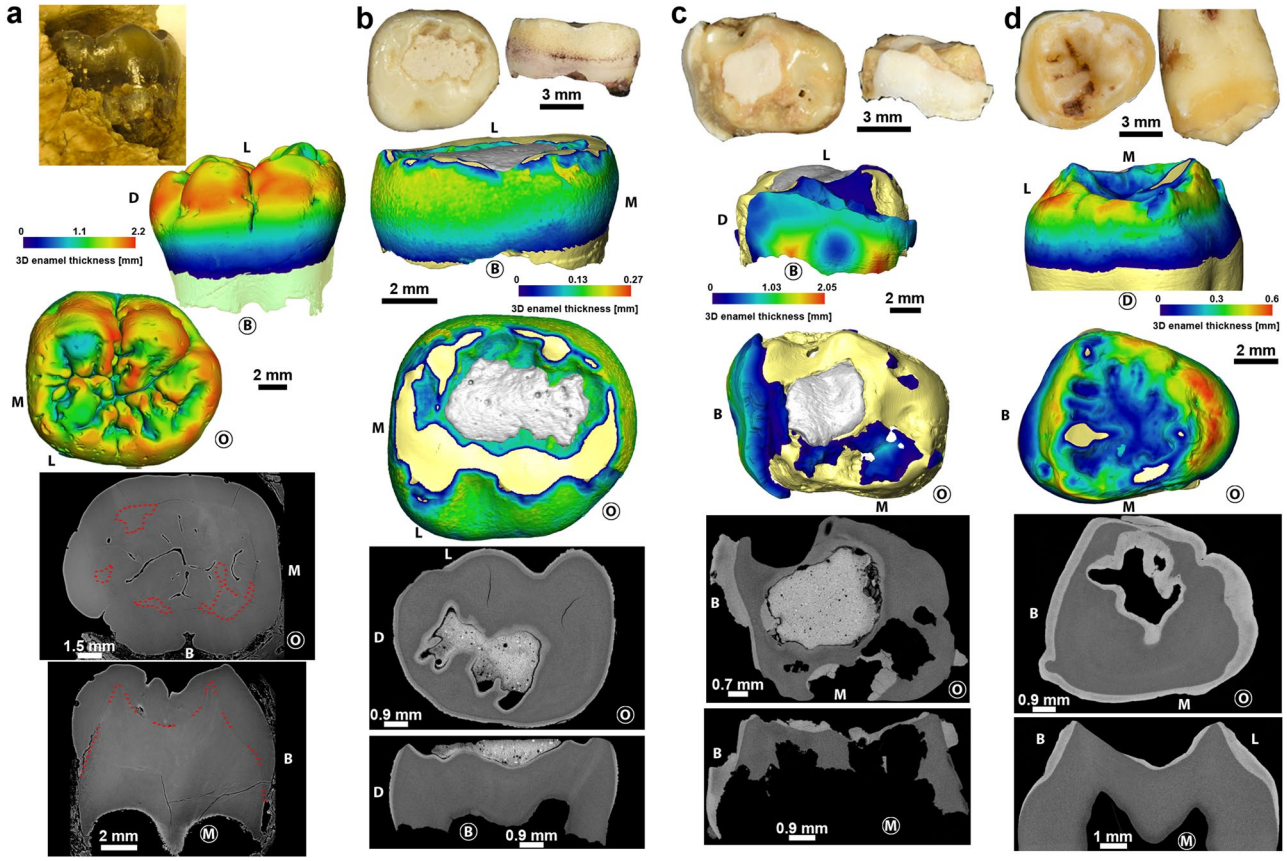

Figure 5. Comparison of the GAR IVE LRM1 (**a**) with three modern human teeth affected by different forms of amelogenesis imperfecta (**b**–**d**; see Supplementary Text S4for details). Photographs (top), 3D enamel thickness maps (middle) and 2D virtual sections (bottom) show that despite the loss of contrast, GAR IVE has a normal enamel thickness and morphology. Anatomical orientation is shows using 'M' for mesial, 'D' for distal, 'B' for buccal, 'L' for lingual and 'O' for occlusal. The side of the tooth in front view is circled.

(i.e., necrophagous insects), which were found to be active at African Plio-Pleistocene sites such as Laetoli and Makapansgat[46,47]. These insects produce various traces, like surface tunnels, pits, and bore holes[48,49]. According to Parkinson[49] the presence of a minimum of three different traces in a fossil assemblage can be used to demonstrate the implication of dermestid beetles. In the faunal assemblage of Layer E, a bone fragment in particular (Fig. 6) shows holes very close in outline and size to the one observed on the GAR IVE juvenile mandible, and thus complies with dermestid beetles activity[50]. Accordingly, dermestid beetles likely fed and developed on the carcasses of animals in close proximity to the bony remains of GAR IVE, and possibly bore pupation chambers into the hominin bone (Supplementary Table S10 and Supplementary Fig. S17), and substantially destroyed the trabecular bone. Following this hypothesis, the insects may have taken advantage of the pre-existing mental foramen, and considerably enlarged it (Figs. 2, 4, Supplementary Text S2).

Relatively large cavities are restricted to the lingual aspect of the surface of the alveolar bone for each erupted deciduous teeth (Fig. 7). These holes are identified as the openings of the gubernacular canals which constitute a guide for the eruptive pathway of the developing permanent tooth germs[51–55]. These gubernacular foramina observed on GAR IVE have a circular diameter ranging from 0.75 mm to 2.46 mm, which is consistent with the standard values[56]. This normal and developmental structure exists in all vertebrates. Smaller pits (~0.15–0.20 mm in diameter) are distributed close to each other on the anterior portion of the mandibular corpus (Fig. 7). The holes are more densely distributed on the buccal aspect than on the lingual side of the bone, close to the anterior border. As seen in 2D virtual sections of the GAR IVE mandibular bone, these holes communicate with larger canals of the vascular system. These holes are foramina called Volkmann's canals which are related to hypervascularisation occurring during normal bone growth and are regularly seen in juveniles[57–59].

Small pits (~0.5 mm in diameter) can also be observed on the teeth and bone of GAR IVE (Fig. 7). They differ from both the previously described gubernacular canals' openings and Volkmann's canals on the bone. Pits can be observed mainly on the enamel surface of the GAR IVE LRM_1. The deciduous molars are very slightly affected with only a couple of pits scattered on the outer enamel surface, and even on the exposed root dentine (Figs. 2, 7). These pits are strictly absent from the LRP_3, LRP_4 and LRC_1 tooth germs, which are enclosed in the alveolar bone and therefore well protected from taphonomic processes. In sharp contrast, both the erupted deciduous teeth, the LRI_2 and the LRM_1, which were partially uncovered post-mortem as a result of a symphysis and ramus fracture, were exposed openly to taphonomic agents. The pits scattered on the bone surface have a more random distribution and are mostly restricted to the posterior half of the mandibular corpus. Interestingly, some of the

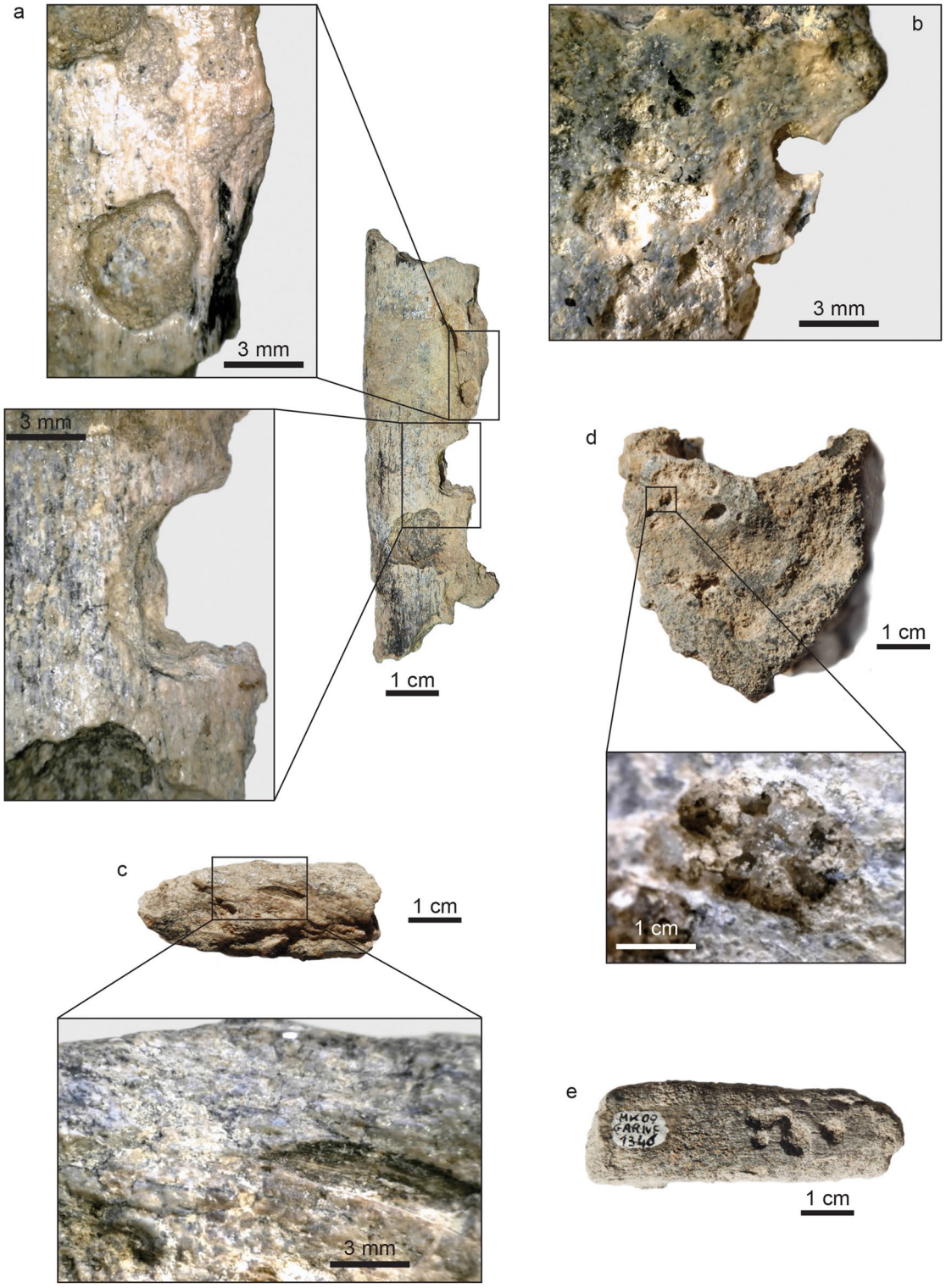

Figure 6. High quality photographs of faunal bone specimens from Garba IVE showing typical modifications left by dermestids. (A) Garba IVE 05-40, Garba IVE 05-57, Garba IVE 05-59, Garba IVE 05-32, Garba IVE 09-1346.

animal bones and teeth of Layer E also display similar pits. The most striking example is a hippopotamus canine with noticeable pits all over its enamel surface (Fig. 8). Therefore, the same taphonomic agent may be held responsible in the case of both hominin and animal remains.

On the lingual side of the mandibular corpus of GAR IVE, four striae point to teeth sharpening by a small rodent (Supplementary Fig. S15), while the posterior portion of the buccal side shows traces of slight weathering

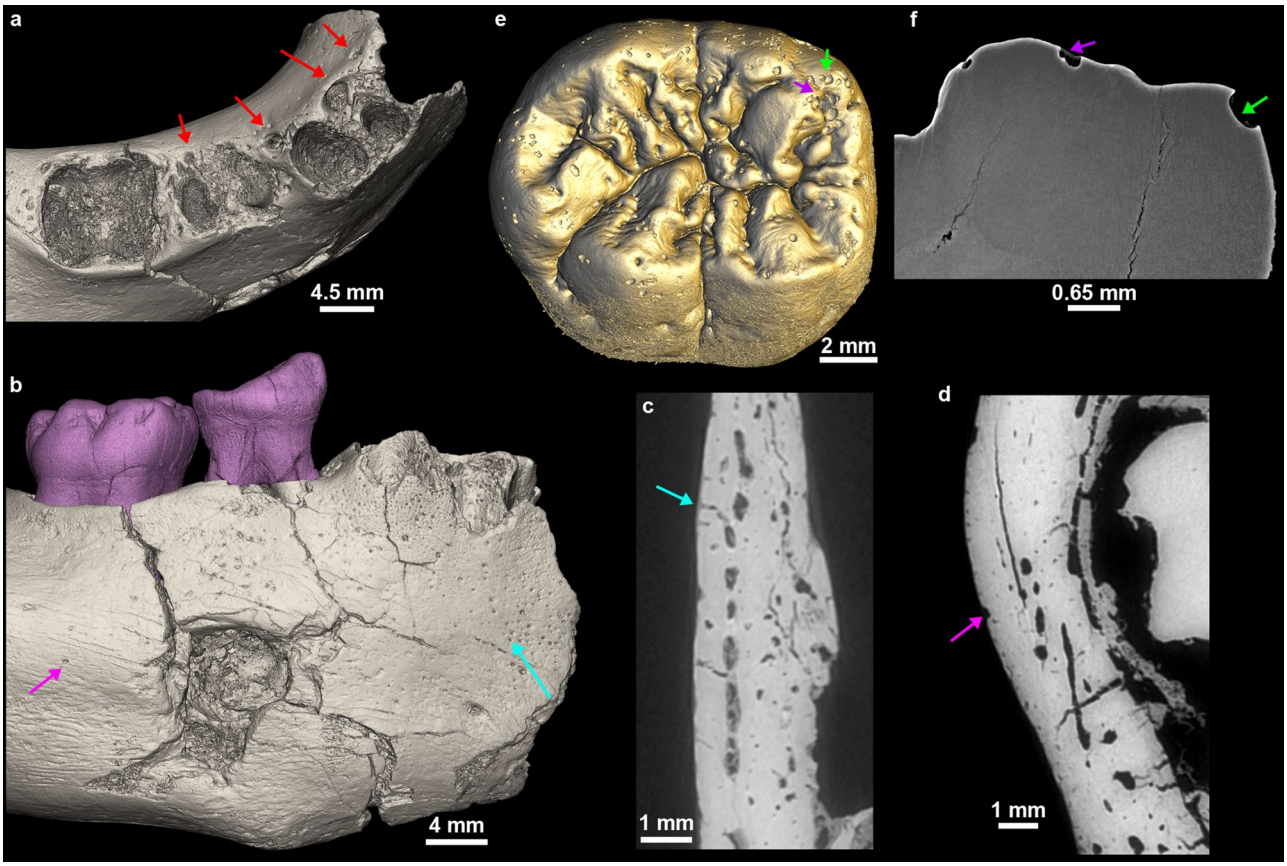

Figure 7. Variety of pits identified on GAR IVE related to the eruption of the permanent germs [gubernacular canals; red arrows on (**a**)], normal bone growth [Volkmann's canals; blue arrow in (**b**) and (**c**)], and of taphonomic origin on the bone [pink arrow in (**b**) and (**d**)] and the teeth [arrows in (**e**) and (**f**)].

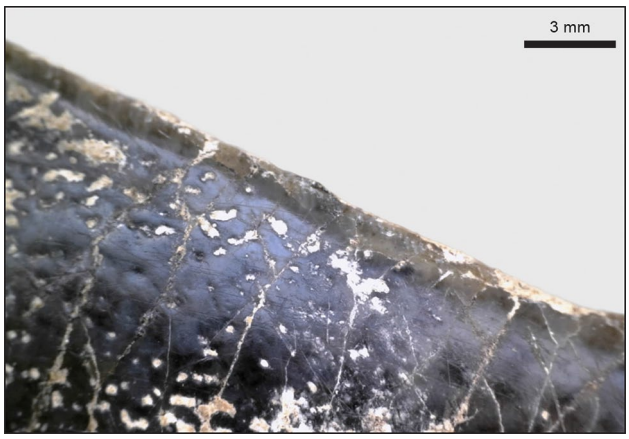

Figure 8. Close-up on the enamel surface of a *Hippopotamus* canine from Garba IVE, showing pits.

(Supplementary Fig. S16). This is further evidence that the corpse of GAR IVE laid exposed and eventually decayed before being buried by alluvial deposits.

These additional surface features cannot be explained either by a pathological condition or by anatomical development. The characteristics of the general environment during fossilization, i.e., taphonomy, were thus considered as potential explanatory variables. They were clarified by the reconstruction of the sedimentary sequence of the Garba IV site where the fossil was unearthed (see Supplementary Text S3 for details). Garba IV is located in a volcanic area which was active during the Early and Middle Pleistocene. In this volcanic environment, chemical corrosion due to water acidity is better accounted for as a general cause of dental tissue alteration

(see Supplementary Text S3 for details). In virtual 2D sections, the edges of the pits observed on the GAR IVE teeth appear sharp and acute (Fig. 7f), reminiscent of, and likely to be, vacuoles of dissolution.

Discussion

Reaching a palaeopathological diagnostic on fossil remains often reveals challenging, even more so as the latter ones are usually fragmentary and damaged. Yet, this has always been attempted, ever since the nineteenth century, with mixed results, e.g., the Neanderthal specimen from Feldhofer Grotte[60]. Trinkaus[40] has recently reviewed published palaeopathological cases, and mentioned GAR IVE and its putative AI as a likely cause for early death. The diagnosis of AI in GAR IVE was based on general enamel dysplasia, the abnormally severe attrition of the deciduous first molar, wrinkling and additional cuspules on the occlusal surfaces of the molars, enamel defects (i.e., shallow pits), as well as reduced enamel radio-opacity[19]. In agreement with Zilberman et al.[19], Trinkaus[40] further concluded that GAR IVE had suffered from restricted functional masticatory capacity resulting from AI, which induced malnutrition around weaning age.

Following Zilberman et al.[19] 's diagnostic, GAR IVE would most likely have been affected by the AI variant called "hypoplastic, pitted autosomal dominant" Type IA as defined by Witkop Jr.[33]. In this variant, enamel may be totally absent or often fragile and significantly thinner to the point of breaking and eventually being totally lost[32, 35, 61]. The enamel surface is often rough, smooth or pitted. This is not the condition observed in GAR IVE: neither preserved deciduous nor permanent teeth are brittle or crumble, partly due to their normal enamel thickness (Fig. 5a, Supplementary Figs. S1 and S19). The inspection of the synchrotron µCT data confirms that the crowns are notably exempt of internal cracks (Figs. 2, 4, Supplementary Fig. S19). This seems to rule out the accumulation of fractures during life, and therefore contributes to the excellent fossilization of the enamel. Only a few cracks could be seen in the roots transversally and may likely have occurred after death. If the teeth had been made fragile during the infant's life by an alteration of the enamel thickness and/or its microstructure, the tooth crowns would have very likely broken off as seen in modern clinical cases[35, 36, 62, 63] (See Fig. 5). By definition, AI should affect enamel formation in all the teeth of both generations[32, 36, 38, 64], which is clearly not the case in GAR IVE. Overall, some kinds of enamel defects may resemble these encountered in AI, although other causes may be identified: either pathological by a differential diagnostic[32] or taphonomic[65] as shown in GAR IVE. Taurodontism is often associated with the hypomaturation form of AI[31, 66]. The deciduous molars' roots of GAR IVE are clearly divergent (Fig. 2), with a normally-sized pulp cavity (the chamber represents one third of the total pulp cavity in height while the root canals extend over the two thirds in height; Supplementary Fig. S1) and thus show no evidence of taurodontism. Accumulation of dental calculus has sometimes been reported in severe forms of AI[66], which is not the case in GAR IVE, although it could have been lost post-mortem.

Severe attrition does not belong to the suite of manifestations defining the hypoplastic forms of AI, but rather in the hypocalcified and hypomaturation AIs. In the latter forms, enamel may prematurely chip away even before tooth emergence[35], which is not the case in GAR IVE.

The extensive wrinkling of the occlusal surface of the GAR IVE LRM_1 (Fig. 3) looks similar to that reported in recent modern humans, in which it is more common on the outer enamel surface than at the enamel-dentine junction, and also in the M_1 than in the dm_2[67, 68]. This morphology has also been observed in several fossil hominin taxa, among which East African robust australopithecines[69]. The occlusal wrinkling of the Omo 427 LRM_2 (Fig. 3) resembles that of GAR IVE, while it is even more pronounced in the Omo 136–1 LLM_3. The LRM_2 of *Australopithecus anamensis* KNM-ER 34725 T is also very similar to GAR IVE (See Fig. 2 in[70]). This supports the hypothesis that this trait is not pathological and rather results from the retention of a primitive morphology in healthy modern humans, and in GAR IVE.

Concerning the pits mainly observed on the enamel surface of the GAR IVE LRM_1, no comparable dental defects could be found in the medical literature. Towle and Irish[71] describe that *Paranthropus robustus* molars show the most frequent occurrence of pitting enamel hypoplasia (PEH) than any other extant Primates studied. They further notice that the pits are more frequent on deciduous than on permanent teeth, the anterior teeth not being affected. Towle and Irish[71] make a correlation between this PEH and the pits observed in modern humans affected by AI, and thus propose that these pits have a genetic origin. If the defects observed on GAR IVE had a genetic and developmental origin, their edges—which were shown to be sharp (Fig. 7)—would have been eroded during the life of the infant due to contact with the saliva and the food items processed in the mouth. Therefore, these enamel alterations may have most likely occurred after death. Additionally, several kinds of pits were also observed on the bone surface, and were interpreted in terms of bone growth (Volkmann canals), tooth development (openings of the gubernacular canals) and taphonomy (See Results).

Some of the clinical criteria commonly used to diagnose AI cannot be reliably used on fossil dental remains, such as the radio-opacity and the coloration of enamel, due to taphonomic processes. The most obvious of them concern changes in enamel colour, which is often used for a differential diagnosis with fluorosis together with enamel flecking and hypoplasias[32]. In fossils, a discolouration of enamel may more likely be related to taphonomic processes[65], as is the case for the very dark enamel of GAR IVE. The argument for the reduced radio-opacity[19] is tricky to consider in fossil teeth as diagenesis may well have altered the original composition of the tooth microstructure. In hypoplastic forms of AI, the contrast between enamel and dentine appears normal radiographically[72]. In GAR IVE, taphonomic processes inducing a remineralization may have altered the coefficient of attenuation of the dental hard tissues to X-rays, thus obscuring its fine enamel microstructure (Figs. 5a, 7f, Supplementary Figs. S1, S19). Only a couple of accentuated lines could be observed in the cuspal enamel of the LRP_4 (See Supplementary Text S1).

Other surface features attest that several taphonomic agents were at play, such as on the posterior portion of the mandibular corpus, where weathering affected the buccal side and rodents sharpened their teeth on the lingual side. The buccal aspect of the mandibular corpus shows a substantial bone loss at the location of the

mental foramen. Zanolli et al.[21] interpreted this cavity as a carnivore tooth mark. The breakage pattern and fissures observed on GAR IVE do not match that resulting from a carnivore bite. To note, that the lingual side of the right mandibular corpus lacks the mark of the counterpart tooth, which may not have systematically imprinted the bone anyways. The size of the hole considerably exceeds that of puncture marks produced by for instance hyenas (Supplementary Fig. S18). Importantly, the high resolution synchrotron scans reveal a virtual 3D negative imprint of the hole showing a convoluted shape, which is little compatible with the shape of a carnivore tooth (Fig. 4). Noteworthy, there are overall very few carnivores in the faunal record of Melka Kunture[24], except the large civet *Pseudocivetta ingens* in Layer E of Garba IV[73] (Supplementary Table S11).

Whether the ontogenetic stage "childhood" has emerged from the *Homo* lineage at ~ 1.8 Ma is still highly debated. There are currently too few juvenile early *Homo* fossils recovered with well-preserved dental and skeletal remains to assess and discuss the pattern and timing of their dental development and skeletal maturation[5]. However several lines of evidence based on dental development studies point to a lack of childhood in early *Homo*. Indeed dental examination of the Nariokotome boy (KNM-WT 15,000, 1.5 Ma) showed that this juvenile, deceased at 8–9 years of age, presented an advanced skeletal and dental maturation suggesting that growth was rapid, with the lack of a slowdown growth characteristic of childhood[11]. KNM-ER 1507 and KNM-ER 820 (See Supplementary Figs. 9 and 10) represent two young *H. erectus* s.l. with an estimated age at death of 5 years[74,75]. Both specimens are more advanced than *P. boisei* specimens in terms of calcification stages[74]. This observation is interesting in light of our comparison of the GAR IVE tooth calcification stages with other fossil hominins, and of the rough estimation of its age at death in comparison with DNH 35 (see Results). The comparison of GAR IVE with modern human equivalents as described by AlQahtani and colleagues[42] show a tremendous variation in mosaic among tooth type (See Supplementary Text S1 and Table S1), likely reflecting a variability in the time of initiation of the germs, and of their rate of calcification. The scoring of each of the GAR IVE teeth after AlQahtani and colleagues[42] provides a range of 3 to 8 years. This is consistent with the results of the Bayesian statistics performed in Zanolli et al.[21], where the calcification sequence of GAR IVE was found in four modern human children aged 2.67, 3.92, 4.54, and 6.42 years. KNM-ER 820 (mandible) has the permanent first molar in occlusion and already worn[74] confirming a rapid growth in this species. Early *Homo* at around 1.5–1.8 Ma would not have experienced any significant period of slow somatic growth between the end of infancy and the juvenile stage[1,11,74–76]. Thompson and Nelson posit that childhood bears a cost to the group of hominins[5]. Although having a stage of childhood decreases child mortality and increase the fertility rate of the mothers, the pressure increases on the whole group to care for the offspring in terms of provisioning and protection during their least productive years of life[5]. Since taphonomy has obscured most the dental microstructure in the GAR IVE teeth, a fine quantitative documentation of the pattern and timing of its dental development remains yet inaccessible. The accentuated lines occurring in some of its tooth germs could have been imprinted by strong stress events occurring before death. It remains however totally speculative to propose that these repeated stress events may have had an impact on the chances of survival of the child, or its health and growth. The circumstances of the death of GAR IVE at a very early stage of its life – presumably before 3 years of age – remains unelucidated. However, our findings proposing that GAR IVE has not suffered from AI restore the status of this early *Homo* infant as not being affected by a pathology which could have been lethal. The tooth morphology of GAR IVE can thus be reliably included in future comparative studies, such as for refining its taxonomic status.

Conclusion

High-resolution synchrotron imaging allowed reassessing the diagnosis of AI in GAR IVE. Among the arguments raised by Zilberman and colleagues[19,30], several cannot be grounded in GAR IVE. We demonstrated that some features interpreted as symptoms of AI are normal anatomical features related to bone growth (i.e., Volkmann's canals) and tooth eruption (i.e., gubernacular canals), while others are resulting from post-mortem process. In general, there is no evidence of a pathological enamel condition in GAR IVE, and all these observations invalidate the diagnosis of AI in this early *Homo* juvenile. GAR IVE can thus be reliably used in future comparative studies as one of the rare early *Homo* infant specimens preserving a partial mixed dentition.

Overall, our results suggest caution when diagnosing a rare genetic disease on a fossil remain, and considering its implications on our understanding of hominin life history and consequently, on human evolution. Fossil human remains gain to be investigated using an integrative approach, combining different fields of expertise, such as taphonomy, environmental reconstruction, archaeological and geological context, high-resolution imaging techniques and/or a clinical approach, whenever needed.

Methods

The GAR IVE mandible is kept in the National Museum of Addis Ababa (Ethiopia) together with the archaeological and palaeontological collections from Garba IV and all other sites of Melka Kunture. ARCCH (Authority for Research and Conservation of the Cultural Heritage) provided the permit for the temporary export of the fossil to be scanned in Grenoble (France) at the European Synchrotron ESRF.

Since the variously-sized and -shaped surface morphology on the GAR IVE teeth had been interpreted as abnormal and lead to reach the general diagnosis of AI, we explored the tooth surface features. Concerning the developmental alterations that AI produces, the analysis of the enamel microstructure is especially valuable. Indeed, dental hard tissues record their own growth and maturation as well as stressful events experienced by the organism[11]. In the enamel, stress events may manifest as accentuated lines which remain non-specific[12–14]. To note that birth is recorded by the neonatal line often identifiable in the enamel and dentine of in deciduous teeth and the mesial cusps of the permanent first molar which start mineralizing *in utero*[15,16].

To access the tooth and bone microstructure of GAR IVE, we scanned the mandible and its dentition at high-resolution using synchrotron propagation phase contrast micro-computed tomography (PPC-SR-µCT).

The scans were acquired by Dr. Paul Tafforeau at the ESRF (Grenoble, France) on the ID 19 beamline. The technical parameters used for the data acquisition are listed in detail in Supplementary Text S4. Two- and three-dimensional techniques of virtual histology were used in VG Studio MAX 3.2 (Volume Graphics, Heidelberg, Germany) to explore the preservation of bone and dental tissues[77].

To reassess the diagnosis of AI in GAR IVE, and further study the 3D enamel thickness distribution in its LRM1, we aimed to access clinical extractions of teeth from patients diagnosed with AI. Despite a wide query in clinical institutions in several countries, we could eventually only access three teeth. The first tooth ("AI_1", (d) in Fig. 5), an ULM3, was collected after extraction indicated by an orthodontic treatment, at the "Centre de référence des maladies rares du métabolisme du phosphore et du calcium" Service d'Odontologie, Hôpital Bretonneau, AP-HP, Paris, France. All teeth were collected with informed and written consent from the patients according to ethical guidelines set by the French law (Loi Bioéthique n°2004–800) and with special ethical authorization for brittle teeth (from the "Comité d'Evaluation de l'Ethique des projets de Recherche Biomédicale (CEERB) Paris Nord" Institutional Review Board -IRB 00,006,477- of GH Nord Université de Paris, AP-HP) and tissue and cell banking agreements (n°DC-2009–927). This female patient was genotyped and was shown to be affected by a mutation on AMELX, which rather argues in favour of an hypoplastic form of AI. The two other teeth are from an historical sample curated in the "Anatomical Collection" of the Department of Oral and Maxillofacial Sciences at the University of La Sapienza, Rome, Italy. Besides the record of that this is a case of AI, there is no further information regarding the deciduous molar "AI_2" ((b) in Fig. 5). According to the historical records of the anatomical collection, the third tooth ("AI_3", (c) in Fig. 5) is an ULdm2 extracted from an 11 year-old girl, who was clinically diagnosed AI. Although there is no more specific information, and due to its brown enamel, it is most probably the hypocalcified form of AI, and potentially the hypocalcified 3A variant after Witkop Jr. (1988). To note that the patients were diagnosed with different forms of AI, with various degrees of certainty and amount of information. We decided to report on the few teeth we had access to, to show a variety of manifestation of putative forms of AI in modern humans. The teeth were scanned on a custom made Diondo D3 µCT-scanner in the Department of Human Evolution, at the MPI-EVA (Leipzig, Germany), and the reconstructed µCT data were analysed in Avizo 7.0 (FEI) (Supplementary Text S4 for further details).

Faunal remains were examined to determine what taphonomic process have been a play at the site, and whether they could have produced the features observed on GAR IVE (e.g., pits on the outer enamel surface) and interpreted as being related to the AI pathology. Taphonomy encompasses the characteristics of the general environment during fossilization. Our approach involved the reconstruction of the palaeonvironmental context of Garba IVE, which is based on the detailed analysis of the stratigraphic sections carried out in 2013 and 2017. Sedimentary features at the meso- and micro-scale (grain size, structure, texture, unconformities) were studied for the reconstruction of the depositional processes, volcanic facies and for correlation with the stratigraphic sections along the Garba and Gombore gully. The results were eventually correlated with the dataset of Raynal and Kieffer[78]. The taphonomic observations conducted on GAR IVE and the associated faunal remains were performed using 10×-20× hand lenses and a Dino-Lite Edge 5MP, at the National Museum, in Addis Ababa, Ethiopia.

Received: 17 May 2021; Accepted: 1 October 2021
Published online: 29 November 2021

References

1. Smith, B. H. Dental development and the evolution of life history in Hominidae. *Am. J. Phys. Anthropol.* **86**, 157–174 (1991).
2. Gurven, M. & Walker, R. Energetic demand of multiple dependents and the evolution of slow human growth. *Proc. R. Soc. B Biol. Sci.* **273**, 835–841 (2006).
3. Hublin, J.-J., Neubauer, S. & Gunz, P. Brain ontogeny and life history in Pleistocene hominins. *Philos. Trans. R. Soc. B Biol. Sci.* **370**, 20140062 (2015).
4. Bogin, B. The evolution of human childhood. *Bioscience* **40**, 1 (1990).
5. Thompson, J. L. & Nelson, A. J. Childhood and Patterns of Growth in the Genus *Homo*. in *Childhood: Origins, Evolution, and Implications* (eds. Meehan, C. L. & Crittenden, A. N.) 75–101 (University of New Mexico Press, 2016).
6. WHO. *Weaning - from breast milk to family food - a guide for health and community workers*. (1988).
7. Fuller, B. T., Richards, M. P. & Mays, S. A. Stable carbon and nitrogen isotope variations in tooth dentine serial sections from Wharram Percy. *J. Archaeol. Sci.* **30**, 1673–1684 (2003).
8. Aiello, L. C. & Wheeler, P. The expensive-tissue hypothesis: the brain and the digestive system in human and primate evolution. *Curr. Anthropol.* **36**, 199–221 (1995).
9. Humphrey, L. T. Weaning behaviour in human evolution. *Semin. Cell Dev. Biol.* **21**, 4 (2010).
10. Neubauer, S. & Hublin, J.-J. The Evolution of Human Brain Development. *Evol. Biol.* **39**, 568–586 (2012).
11. Dean, M. C. & Smith, B. H. Growth and development of the Nariokotome youth, KNM-WT 15000. in *The First Humans - Origin Early Evolution of the Genus Homo* (eds. Grine F.E., Fleagle J.G., Leakey R.E.) Vertebrate Paleobiology and Paleoanthropology. 101–120 (Springer, Dordrecht, 2009).
12. Goodman, A. H. & Rose, J. C. Assessment of systemic physiological perturbations from dental enamel hypoplasias and associated histological structures. *Am. J. Phys. Anthropol.* **33**, 59–110 (1990).
13. Schwartz, G. T., Reid, D. J., Dean, M. C. & Zihlman, A. L. A faithful record of stressful life events recorded in the dental developmental record of a juvenile gorilla. *Int. J. Primatol.* **27**, 1201–1219 (2006).
14. Birch, W. & Dean, M. C. A method of calculating human deciduous crown formation times and of estimating the chronological ages of stressful events occurring during deciduous enamel formation. *J. Forensic Leg. Med.* **22**, 127–144 (2014).
15. Zanolli, C., Bondioli, L., Manni, F., Rossi, P. & Macchiarelli, R. Gestation length, mode of delivery, and neonatal line-thickness variation. *Hum. Biol.* **83**, 695–713 (2011).
16. Dean, M. C., Spiers, K. M., Garrevoet, J. & Le Cabec, A. Synchrotron X-ray fluorescence mapping of Ca, Sr and Zn at the neonatal line in human deciduous teeth reflects changing perinatal physiology. *Arch. Oral Biol.* **104**, 90–102 (2019).
17. Joannes-Boyau, R. *et al.* Elemental signatures of *Australopithecus africanus* teeth reveal seasonal dietary stress. *Nature* **572**, 112–115 (2019).

18. Tacail, T. *et al.* Calcium isotopic patterns in enamel reflect different nursing behaviors among South African early hominins. *Sci. Adv.* **5**, eaax3250 (2019).
19. Zilberman, U., Smith, P., Piperno, M. & Condemi, S. Evidence of amelogenesis imperfecta in an early African *Homo erectus*. *J. Hum. Evol.* **46**, 647–653 (2004).
20. Condemi, S. The Garba IV E mandible. in *Studies on the Early Paleolithic site of Melka Kunture, Ethiopia* (eds. Chavaillon, J. & Piperno, M.) 687–701 (2004).
21. Zanolli, C. *et al.* Structural organization and tooth development in a *Homo* aff. *erectus* juvenile mandible from the Early Pleistocene site of Garba IV at Melka Kunture, Ethiopian highlands. *Am. J. Phys. Anthropol.* **162**, 533–549 (2017).
22. Semaw, S. *et al.* Co-occurrence of Acheulian and Oldowan artifacts with *Homo erectus* cranial fossils from Gona, Afar, Ethiopia. *Sci. Adv.* **6**, eaaw4694 (2020).
23. Gallotti, R. Before the Acheulean in East Africa: An Overview of the Oldowan Lithic Assemblages. in *The Emergence of the Acheulean in East Africa and Beyond: Contributions in Honor of Jean Chavaillon* (eds. Gallotti, R. & Mussi, M.) 13–32 (Springer International Publishing, Berlin, 2018). https://doi.org/10.1007/978-3-319-75985-2_2.
24. Geraads, D., Eisenmann, V. & Petter, G. The Large Mammal Fauna of the Oldowayan sites of Melka-Kunturé, Ethiopia. in *Studies on the Early Paleolithic site of Melka Kunture, Ethiopia.* (eds. Chavaillon, J. & Piperno, M.) 169–192 (2004).
25. Piperno, M. & Bulgarelli, G. M. The site of Garba IV. Excavations 1973–1982. in *Studies on the Early Paleolithic site of Melka Kunture, Ethiopia* (eds. Chavaillon, J. & Piperno, M.) 449–458 (2004).
26. Morgan, L. E. *et al.* A chronological framework for a long and persistent archaeological record: Melka Kunture, Ethiopia. *J. Hum. Evol.* **62**, 104–115 (2012).
27. Gallotti, R. & Mussi, M. The Unknown Oldowan: ~1.7-Million-Year-Old Standardized Obsidian Small Tools from Garba IV, Melka Kunture, Ethiopia. *PLOS ONE* **10**, e0145101 (2015).
28. Bonnefille, R., Melis, R. T. & Mussi, M. Variability in the Mountain Environment at Melka Kunture Archaeological Site, Ethiopia, During the Early Pleistocene (~1.7 Ma) and the Mid-Pleistocene Transition (0.9–0.6 Ma). in *The Emergence of the Acheulean in East Africa and Beyond: Contributions in Honor of Jean Chavaillon* (eds. Gallotti, R. & Mussi, M.) 93–114 (Springer International Publishing, Berlin, 2018). https://doi.org/10.1007/978-3-319-75985-2_5.
29. Raynal, J.-P., Kieffer, G. & Bardin, G. Garba IV and the Melka Kunture Formation. A preliminary lithostratigraphic approach. in *Studies on the Early Paleolithic site of Melka Kunture, Ethiopia.* (eds. Chavaillon, J. & Piperno, M.) 137–166 (2004).
30. Zilberman, U., Smith, P. & Condemi, S. Evidence for a genetic disorder affecting tooth formation in the Garba IV child. in *Studies on the Early Paleolithic site of Melka Kunture, Ethiopia* (eds. Chavaillon, J. & Piperno, M.) 703–713 (2004).
31. Wright, J. T. The molecular etiologies and associated phenotypes of amelogenesis imperfecta. *Am. J. Med. Genet. A.* **140A**, 2547–2555 (2006).
32. Crawford, P. J., Aldred, M. & Bloch-Zupan, A. Amelogenesis imperfecta. *Orphanet J. Rare Dis.* **2**, 17 (2007).
33. Witkop, C. J. Jr. Amelogenesis imperfecta, dentinogenesis imperfecta and dentin dysplasia revisited: problems in classification. *J. Oral Pathol. Med.* **17**, 547–553 (1988).
34. Aldred, M., Savarirayan, R. & Crawford, P. Amelogenesis imperfecta: a classification and catalogue for the 21st century. *Oral Dis.* **9**, 19–23 (2003).
35. Prasad, M. K., Laouina, S., Alloussi, M. E., Dollfus, H. & Bloch-Zupan, A. Amelogenesis Imperfecta: 1 Family, 2 Phenotypes, and 2 Mutated Genes. *J. Dent. Res.* **95**, 1457–1463 (2016).
36. Sabandal, M. M. I. & Schäfer, E. Amelogenesis imperfecta: review of diagnostic findings and treatment concepts. *Odontology* **104**, 245–256 (2016).
37. Bardet, C. *et al.* Claudin-16 deficiency impairs tight junction function in ameloblasts, leading to abnormal enamel formation. *J. Bone Miner. Res.* **31**, 498–513 (2016).
38. Smith, C. E. L. *et al.* Amelogenesis Imperfecta; Genes, Proteins, and Pathways. *Front. Physiol.* **8**, 435 (2017).
39. Zanolli, C., Hourset, M., Esclassan, R. & Mollereau, C. Neanderthal and Denisova tooth protein variants in present-day humans. *PLoS ONE* **12**, e0183802 (2017).
40. Trinkaus, E. An abundance of developmental anomalies and abnormalities in Pleistocene people. *Proc. Natl. Acad. Sci.* **115**, 11941 (2018).
41. Maples, W. R. Trauma analysis by the forensic anthropologist. in *Forensic osteology: advances in the identification of human remains* (ed. Reichs, K. J.) 218–228 (Charles C. Thomas Springfield, IL, 1986).
42. AlQahtani, S. J., Hector, M. P. & Liversidge, H. M. Brief communication: the London atlas of human tooth development and eruption. *Am. J. Phys. Anthropol.* **142**, 481–490 (2010).
43. Kuykendall, K. L. Dental development in chimpanzees (*Pan troglodytes*): The timing of tooth calcification stages. *Am. J. Phys. Anthropol.* **99**, 135–157 (1996).
44. Dean, C. *et al.* Growth processes in teeth distinguish modern humans from *Homo erectus* and earlier hominins. *Nature* **414**, 628–631 (2001).
45. Smith, T. M. *et al.* Dental ontogeny in pliocene and early pleistocene hominins. *PLoS ONE* **10**, e0118118 (2015).
46. Kitching, J. W. On some fossil arthropoda from the Limeworks, Makapansgat, Potgietersrus. *Palaeontol. Afr.* **23**, 63–68 (1980).
47. Kaiser, T. M. & Katterwe, H. The application of 3D-microprofilometry as a tool in the surface diagnosis of fossil and sub-fossil vertebrate hard tissue. An example from the Pliocene Upper Laetolil Beds, Tanzania. *Int. J. Osteoarchaeol.* **11**, 350–356 (2001).
48. Britt, B. B., Scheetz, R. D. & Dangerfield, A. A suite of dermestid beetle traces on dinosaur bone from the Upper Jurassic Morrison Formation, Wyoming, USA. *Ichnos* **15**, 59–71 (2008).
49. Parkinson, A. H. *Dermestes maculatus* and *Periplaneta americana*: bone modification criteria and establishing their potential as climatic indicators (M. Sc. thesis, University of the Witwatersrand, 2012).
50. Martin, L. D. & West, D. L. The recognition and use of dermestid (Insecta, Coleoptera) pupation chambers in paleoecology. *Palaeogeogr. Palaeoclimatol. Palaeoecol.* **113**, 303–310 (1995).
51. Delabarre, C. F. Dissertation sur l'histoire des dents. (1806).
52. Delabarre, C. F. *Traité de la seconde dentition et méthode naturelle de la diriger; suivis d'un Aperçu de séméiotique buccale.* (1819).
53. Serres, E. R. A. *Essai sur l'anatomie et la physiologie des dents, ou, Nouvelle théorie de la dentition.* (Méquignon-Marvis, 1817).
54. Malassez, M. Sur la structure du *gubernaculum dentis* et la théorie paradentaire. *Comptes Rendus Séances Société Biol. Ses Fil.* **4**, 416–418 (1887).
55. Hodson, J. The gubernaculum dentis. *Dent. Pract. Dent. Rec.* **21**, 423 (1971).
56. Chaudhry, A. & Sobti, G. Visualization of Gubernacular Tract of Transmigrated Canine on CBCT. *J. Evol. Med. Dent. Sci.* **8**, 3637–3641 (2019).
57. Jaffe, H. L. The vessel canals in normal and pathological bone. *Am. J. Pathol.* **5**, 323–337 (1929).
58. Dempster, W. T. & Enlow, D. H. Patterns of vascular channels in the cortex of the human mandible. *Anat. Rec.* **135**, 189–205 (1959).
59. Kingsmill, V. J., Gray, C. M., Moles, D. R. & Boyde, A. Cortical Vascular Canals in Human Mandible and Other Bones. *J. Dent. Res.* **86**, 368–372 (2007).
60. Virchow, R. Untersuchung des Neanderthal-Schädels. *Z. Für Ethnol.* **4**, 157–165 (1872).
61. Achmad, H., Thahir, H. & Adam, M. Amelogenesis imperfecta in children: review of pathogenetic aspect. *Int. J. Sci. Res.* **6**, 2366–2370 (2017).

62. Chanmougananda, S. C., Ashokan, K. A., Ashokan, S. C., Bojan, A. B. & Ganesh, R. M. Literature review of amelogenesis imperfecta with case report. *J. Indian Acad. Oral Med. Radiol.* **24**, 83 (2012).
63. Anitha, M., Sathvikalakshmi, B., Khan, A. F. & Sudharshan, R. Amelogenesis imperfecta–3 cases. *J. Adv. Med. Pharm. Sci.* **17**, 1–8 (2018).
64. Rajshekar, M., Mithun, T., Idiculla, J. J. & Tennant, M. Developmental anomalies of teeth and their applications in forensic odontology. *Eur. J. Forensic Sci.* **3**, 39 (2016).
65. Garot, E., Couture-Veschambre, C., Manton, D. J., Bekvalac, J. & Rouas, P. Differential diagnoses of enamel hypomineralisation in an archaeological context: A postmedieval skeletal collection reassessment. *Int. J. Osteoarchaeol.* **29**, 747–759 (2019).
66. Bäckman, B. Amelogenesis imperfecta: an epidemiologic, genetic, morphologic and clinical study. (Departments of Pedodontics and Oral Pathology at the University of Umeå, 1989).
67. Korenhof, C. A. W. Remnants of the trigonid crests in medieval molars of man of Java. in *Development, Function, and Evolution of Teeth.* (eds. Butler, P.M. & Joysey K.) 157–170 (Academic Press, Cambridge, 1978).
68. Smith, P., Koyoumdjisky-Kaye, E., Kalderon, W. & Stern, D. Directionality of dental trait frequency between human second deciduous and first permanent molars. *Arch. Oral Biol.* **32**, 5–9 (1987).
69. Ramirez Rozzi, F. V. Tooth development in East African *Paranthropus*. *J. Hum. Evol.* **24**, 429–454 (1993).
70. Skinner, M. M., Alemseged, Z., Gaunitz, C. & Hublin, J.-J. Enamel thickness trends in Plio-Pleistocene hominin mandibular molars. *J. Hum. Evol.* **85**, 35–45 (2015).
71. Towle, I. & Irish, J. D. A probable genetic origin for pitting enamel hypoplasia on the molars of *Paranthropus robustus*. *J. Hum. Evol.* **129**, 54–61 (2019).
72. Gadhia, K., McDonald, S., Arkutu, N. & Malik, K. Amelogenesis imperfecta: an introduction. *Br. Dent. J.* **212**, 377–379 (2012).
73. Geraads, D. Faunal Change in Eastern Africa at the Oldowan – Acheulean Transition. in *The Emergence of the Acheulean in East Africa and Beyond: Contributions in Honor of Jean Chavaillon* (eds. Gallotti, R. & Mussi, M.) 183–194 (Springer International Publishing, Berlin, 2018). https://doi.org/10.1007/978-3-319-75985-2_9.
74. Dean, M. C. The dental developmental status of six East African juvenile fossil hominids. *J. Hum. Evol.* **16**, 197–213 (1987).
75. Bromage, T. G. & Dean, M. C. Re-evaluation of the age at death of immature fossil hominids. *Nature* **317**, 525–527 (1985).
76. Dean, M. C. Measures of maturation in early fossil hominins: events at the first transition from australopiths to early *Homo*. *Philos. Trans. R. Soc. B Biol. Sci.* **371**, (2016).
77. Le Cabec, A., Tang, N. K. & Tafforeau, P. Accessing developmental information of fossil hominin teeth using new synchrotron microtomography-based visualization techniques of dental surfaces and interfaces. *PLoS ONE* **10**, e0123019 (2015).
78. Raynal, J.-P. & Kieffer, G. Lithology, dynamism and volcanic successions at Melka Kunture (Upper Awash, Ethiopia). in *Studies on the Early Paleolithic site of Melka Kunture, Ethiopia* (eds. Chavaillon, J. & Piperno, M.) 111–135 (2004).

Acknowledgements

We are grateful to the Authority for Research and Conservation of the Cultural Heritage and to the Ministry of Culture and Tourism of the Federal Republic of Ethiopia for the loan and temporary export permit of MK 81 GAR IVE 0043 (November 27, 2015-January 26, 2016) awarded to Prof. M. Mussi. We thank Dr. Guy Barnish, Dr. Kristiaan D'Aout, Prof. M. Christopher Dean, Dr. Luca Di Bianco, Dr. Martin Donnelly, Dr. Robin Feeney, Justin Honeyford, Dr. James La Course, Dr. Christopher Lynch, Prof. Robin O'Sullivan, Colonel Lucio Redi, Dr. Paul Tafforeau and the ESRF staff on the ID19 beamline, Dr. Zewdi Tsegai, Silke Streiber, Dr. Frido Welker and Dr. Paul Zaslansky. This research is supported by Università di Roma Sapienza, the Italian Ministry of Foreign Affairs, the Max Planck Society, the European Synchrotron (ESRF), the CNRS, the GPR (Grand Programme de Recherche) "Human Past" of the University of Bordeaux's Initiative d'Excellence, and the Römisch-Germanisches Zentralmuseum, Leibniz-Research-Institute for Archaeology. Finally, we thank Wu Liu (Editorial Board Member), and two anonymous reviewers who provided very constructive and helpful comments to improve this manuscript.

Author contributions

M.M. and A.L.C. conceived the research. A.L.C. analysed the synchrotron micro-CT scans. A.L.C., T.C., F.R.R., C.C., M.M., J.-J.H. and G.D.C. discussed the consequences of the reassessment of the pathology diagnosed on the fossil, with regards to life history in early *Homo*. S.G.-W. and D.C. investigated the potential action of taphonomic agents on the GAR-IVE mandible through the comparative study of the faunal remains found at Garba (S.G.-W.) and modern experimental forensic studies (D.C.). L.P., R.M. and M.M. characterized the geology and described the process of formation of the Garba site. A.L.C., F.R.R. and M.M. wrote the manuscript, with contributions from all the co-authors.

Funding

Open Access funding enabled and organized by Projekt DEAL.

Competing interests

The authors declare no competing interests.

Additional information

Supplementary Information The online version contains supplementary material available at https://doi.org/10.1038/s41598-021-02462-1.

Correspondence and requests for materials should be addressed to A.L.C. or M.M.

SUPPLEMENTARY INFORMATION

Insights into the palaeobiology of an early *Homo* infant: multidisciplinary investigation of the GAR IVE hemi-mandible, Melka Kunture, Ethiopia.

A. Le Cabec, T. Colard, D. Charabidze, C. Chaussain, G. Di Carlo, S. Gaudzinski-Windheuser, J.-J. Hublin, R. T. Melis, L. Pioli, F. Ramirez-Rozzi, M. Mussi.

Contents

1. Estimating the age of the stress events in LRP4 enamel. (Suppl. Text S1)

1.1. Estimating GAR IVE's age at death using modern standards

Virtual developmental sections were recorded in each tooth to assess its stage of formation (e.g., [1]). Since the inner structure of the teeth was obscured by taphonomic alterations, the EDJ was drawn in colour after close inspection of the scans to facilitate the assessment and the scoring of the developmental stages (Suppl. Fig. S1).

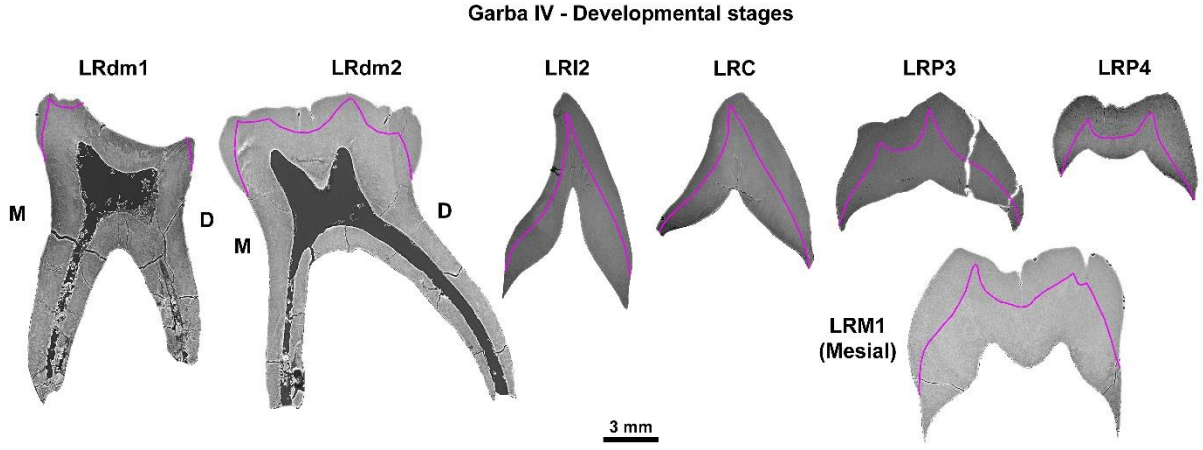

Supplementary Figure S1 – Virtual developmental 2D sections through the GAR IVE deciduous and permanent teeth. Due to the lack of contrast, the EDJ was delineated in pink to facilitate the visualisation of the enamel and dentine thickness.

To note that the I_2 has developed 1.5 mm of root on the lingual aspect, and ~2 mm of root on the buccal aspect, the P_3 has formed 0.6 mm on both sides, and the M1 has

formed 2.6 mm of root on its lingual aspect, for 3.8 mm on the lingual side of its mesial section.

1.1.1. Recent modern humans

Based on radiographs, Condemi[2] had estimated GAR IVE's age to fall between 3 and 4 years. Zanolli et al.[3] refined this estimation at 2.5-3.5 years.

After inspection of the PPC-SR µCT data (Suppl. Fig. S1), the calcification stages were scored and corresponding median ages were listed per tooth type after the modern human atlas built by AlQahtani et al.[4] (Suppl. Table S1).

Mandibular tooth type	dm1	dm2	I2	C	P3	P4	M1
Score for tooth formation stage (after Fig. 1 in AlQahtani et al.[4])	Ac to Res1/4	At least Rc	R1/4	~CrC	Ri	Cr1/2	R1/4
Median corresponding age (years)	8‡	3*	5.5†	5.5†	7.5‡	5†	5.5†

*: from Table 4 ; †: from Table 5; ‡: from Table 6 in AlQahtani et al.[4].

Supplementary Table S1 – Scoring of the calcification stages of GAR IVE, and estimated corresponding age in modern human standards after AlQahtani et al. (2010)[4].

The overall pattern of GAR IVE would be equivalent to **4.5 years** in modern human equivalent after Fig. 6 in AlQahtani et al. (2010)[4] (Suppl. Fig. S2)

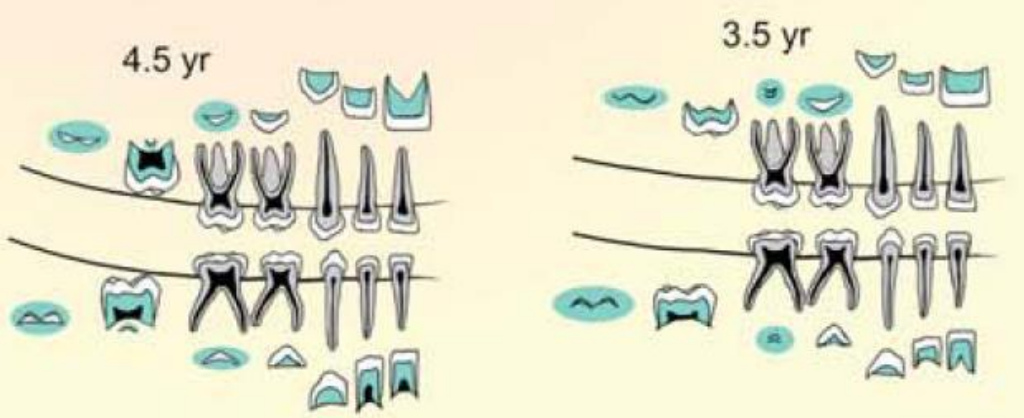

Supplementary Figure S2 – Modern human developmental stages closest to GAR IVE, with a higher match with the 4.5 years schematic (modified after Figure 6 in AlQahtani et al., 2010 [4]).

1.1.2. Chimpanzees

Kuykendall[5] designed a scoring system based on Demirjian and colleagues[6] for exploring chimpanzee dental development. From the collected data on these known age specimens, he built a regression model to calculate a developmental age. Kuykendall [5]'s equation is as follows:

$$Age = 0.078Dm + 0.002\ Dm^2 - 0.073 \pm 0.99$$

Where "Dm" is the sum of the individual scores for a quadrant of the mandibular dentition (in this equation, omitting the M3).

This scoring system is often used to estimate a chimpanzee-equivalent age for fossil hominins (e.g., [7,8]).

In GAR IVE, the LRI1 is not preserved but is assumed to be at least at a stage equivalent to that of the LRI2. The LRM2 is also missing, but since its initiation is likely very close in time to that of the LRP4, their developmental stage is assumed to be the same.

Tooth type (mandibular right quadrant)	I1	I2	C	P3	P4	M1	M2	Dm
Kuykendall (1996) score	5	5	4	4	3	5	3	29

Supplementary Table S2 – Scoring of the calcification stages of GAR IVE after Kuykendall (1996)[5].

The sum of these scores is Dm = 29 (Suppl. Table S2). This yields a "chimpanzee-equivalent" age of 3.87 years with a range of 2.88 – 4.86 years.

Yet, since Kuykendall[5]'s scoring was designed on radiographs and that we score on µCT data, the regression underestimates the stage of development of the germs. We apply the conversion system designed in Gunz et al. [8] on the above radiographic stages to take into account the µCT data:

	I1	I2	C	P3	P4	M1	M2	Dm
Scores on µCT	4.5	4.5	3.5	4.5	3.5	4.5	3.5	
Converted Kuykendall scores	4	4	3	4	3	4	3	25

Supplementary Table S3 – Scoring of the calcification stages of GAR IVE after converting the Kuykendall (1996)[5] scores from the use of µCT data after Gunz et al. (2020)[8].

The new sum of these converted scores is Dm = 25 (Suppl. Table S3), leading to a new age and range estimate : ***3.13 [2.14 – 4.12] years***.

1.2. Early hominins of similar dental developmental stage

Several early hominins show a stage of dental development similar to that of GAR IVE, some of which have a published histological age at death[7,9]. The stage of development of the M1 roots and of the P4 are of special interest.

-*P. boisei* KNM-ER 1477: 2.5-3.0 years [9].

Fig. 1 Occlusal view of juvenile mandible KNM-ER 1477.

Supplementary Figure S3 – Photograph of the occlusal aspect of KNM-ER 1477 (After Fig. 1 in Leakey, 1973[10]). See Fig. 1 in Dean, 1987[9] for periapical radiographs of the developing teeth of KNM ER 1477.

KNM-ER 1477 (Suppl. Fig. S3, and Fig. 1 in Dean, 1987[9]) is slightly less advanced than GAR IVE as its M1 has achieved crown formation but has yet not initiated root formation. The C, P3 and P4 are still developing their crown, with P3 being more advanced than P4.

-*P. boisei* KNM-ER 812: 2.5-3.0 years [9].

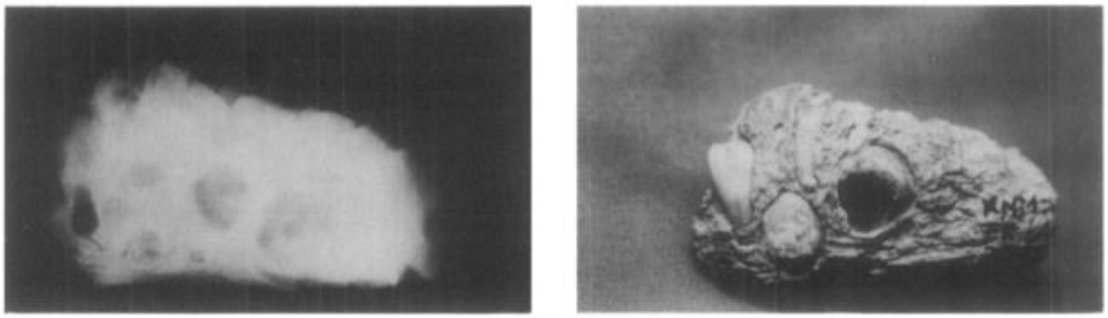

Figure 2. Radiograph of specimen KNM ER 812 together with a photograph of the specimen, (buccal aspect) that also demonstrates the exposed developing permanent teeth.

Supplementary Figure S4 – Radiograph and photograph of KNM-ER 812 (after Fig. 2 in Dean, 1987 [9]).

KNM-ER 812 (Suppl. Fig. S4) seems to overall follow the same pattern and timing of dental development. Besides the preserved roots of the deciduous canine and molars, I1 has completed its crown and has already formed ~2mm of root. The I2 is slightly less advanced. The canine crown is still developping. P3 and P4 are still forming their cuspal enamel. M1 has complete crown and started root formation.

-*P. boisei* KNM-ER 1820: 2.5-3.1 years [9].

In the left mandibular corpus of KM-ER 1820 (Suppl. Fig. S5), the I1 has formed >2mm of root, the canine and P4 crowns are developing, while the P3 has completed its cuspal enamel. The M1 has started forming its roots although the furcation level has not been attained yet. This makes it slightly more advanced than GAR IVE.

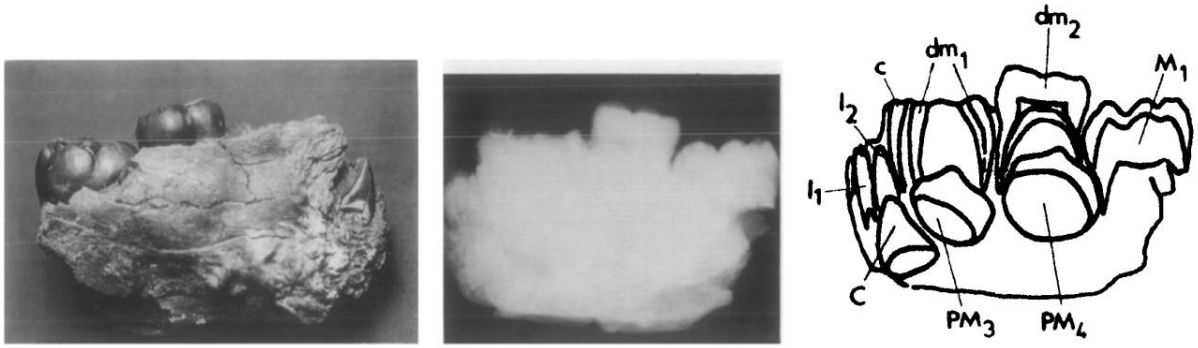

Figure 3. Radiograph of specimen KNM ER 1820 together with a tracing of the developing teeth as seen on the original X ray film and a photograph of the lingual aspect of the specimen.

Supplementary Figure S5 – Photograph and radiograph of KNM-ER 1820 (after Fig. 3 in Dean, 1987 [9]).

- *A. anamensis* KNM-KP 31712: 2.8 years [7].

KNM-KP 31712 shows the same developmental stage as GAR IVE for both the permanent canine and M1 (Suppl. Fig. S6).

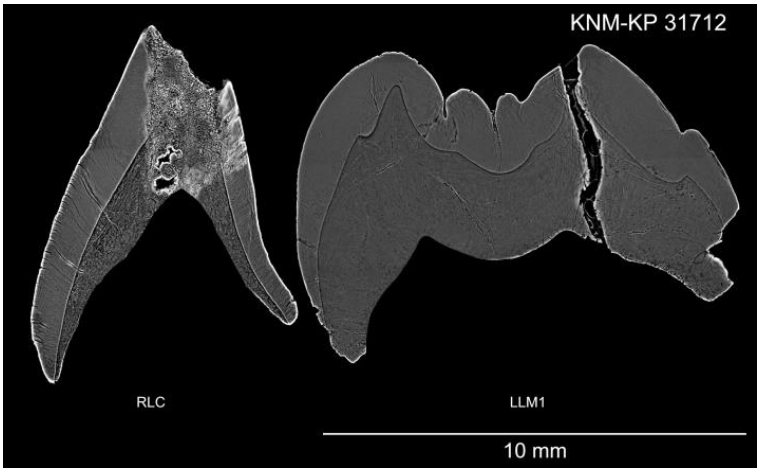

Supplementary Figure S6 –Virtual 2D section through the developmental plane the LRC and LLM1 of *A. anamensis* specimen KNM-ER 812 (after Fig. C in S1 file of Smith et al., 2015[7]).

- *P. robustus* SK 62: 3.12 years [7].

Supplementary Figure S7 –Virtual 2D section through the developmental plane the permanent tooth germs of *P. robustus* specimen SK 62 (after Fig. H in S1 file of Smith et al., 2015[7]).

Compared to SK62 (Suppl. Fig. S7), GAR IVE has a similar stage for its M1 and C. Yet, SK62‘s incisors are much more advanced (almost reaching half of the root formation). GAR IVE’s P4 is more advanced.

-*P. boisei* OH 30: 2.7-3.2 years [9].

OH 30 consists in isolated teeth[9]: 3 deciduous teeth and 13 developing permanent teeth with virtually no root formed yet (no photo nor radiographs). The I1 is just complete while the I2 and C crowns are still forming. The M1s have completed crown formation and, in some places, 1 mm of root can be observed. The P3 and P4 have finished forming their cuspal enamel.

- *A. africanus* Sts 24: 4.35 years [7].

GAR IVE is developmentally less advanced than Sts 24 (Suppl. Fig. S8), especially regarding its M1 root which has not formed until the furcation level. In Sts 24, the C, P3 and P4 are at similar stages than in GAR IVE. To note that GAR IVE's I2 is more advanced in having initiated its root formation.

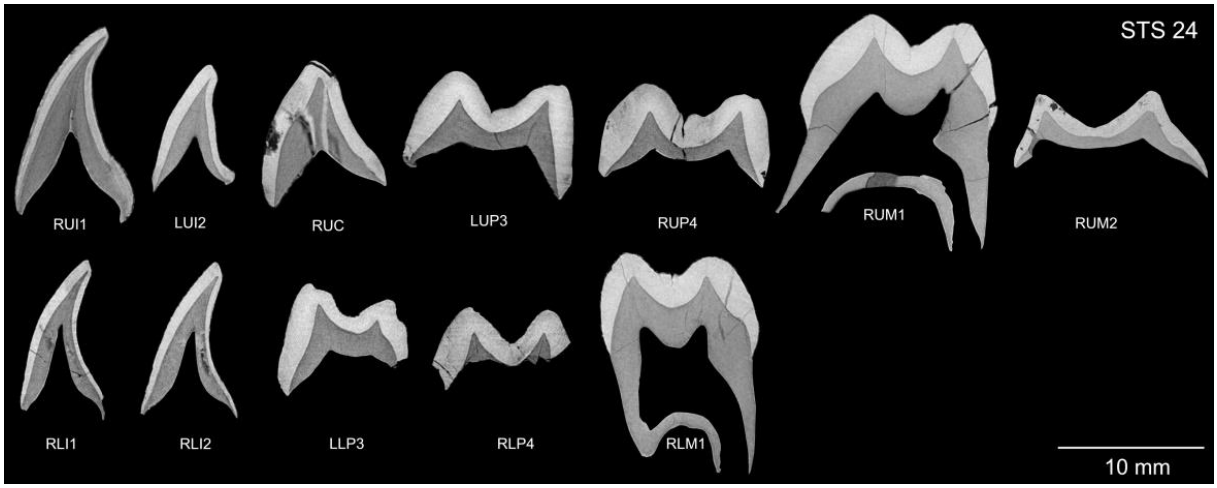

Supplementary Figure S8 –Virtual 2D section through the developmental plane the permanent tooth germs of *A. africanus* specimen Sts 24 (after Fig. F in S1 file of Smith et al., 2015[7]).

- Early *Homo* KNM-ER 820 : 5.3 years[11], and KNM-ER 1507[9].

For both early *Homo* specimens, no histological age at death was estimated, yet, base don perikymata counts on an I_2 and an estimated age of initiation, KNM-ER 820 was estimated to be 5.3 years[11]. The following descriptions follow the data provided by Dean (1987)[9].

KNM-ER 820 (Suppl. Fig. S9) is a fairly complete mandible with a mixed dentition. The four deciduous molars are preserved although worn because in functional occlusion. The deciduous canines are slightly less well preserved. Among permanent teeth, 6 are erupted, 8 are still in their crypt. The central incisors are worn to the dentine with root apices still open. Both I_2 show minimal wear and also have their root apex open. The canines and the premolars are at a similar calcification stage, with 3.6 mm and 4-5 mm of root developped, respectively. The M_1s are in occlusion, with the dnetine horns of the mesio-buccal cusp exposed, and the root apices open. The M_2 are not emerged although they have completed their crown and started root formation. The M3 are not formed yet, i.e., the crypt is visible but no cusp could be identified on the radiographs.

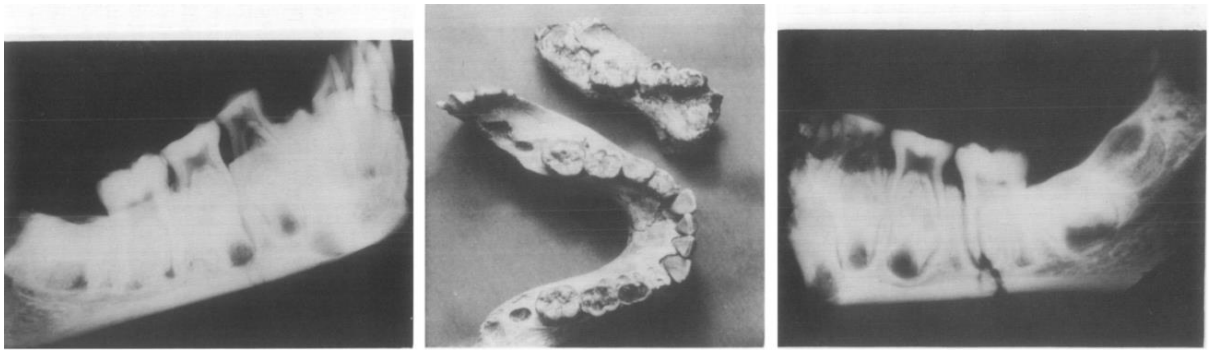

Figure 4. Radiographs of the left and right mandibular corpora of specimen KNM ER 820 together with a photograph of specimens KNM ER 820 and 1507 side by side for comparison.

Supplementary Figure S9 – Radiograph of the right (left) and right (left) side of the mandible of early *Homo* KNM-ER 820. Photograph (middle) of this specimen besides the early *Homo* fragmentary mandible KNM-ER 1507 (after Fig. 4 in Dean, 1987[9]).

KNM-ER 1507 (Suppl. Fig. S10) is a fragment of left mandible preserving 3 erupted teeth (dm_1, dm_2, and M_1) and 4 developping teeth in their crypt (C, P_3, P_4, M_2). The canine has 2.5 mm of root formed, the M_1 is in occlusion, already slightly worn and its root apices are still open. The P_3 has completed crown formation and has developped 2 mm of root. The P_4 is at a slightly less advanced stage of development. The M_2 is at a stage of calcification similar to the P_3, with 1.5-2 mm of root formed.

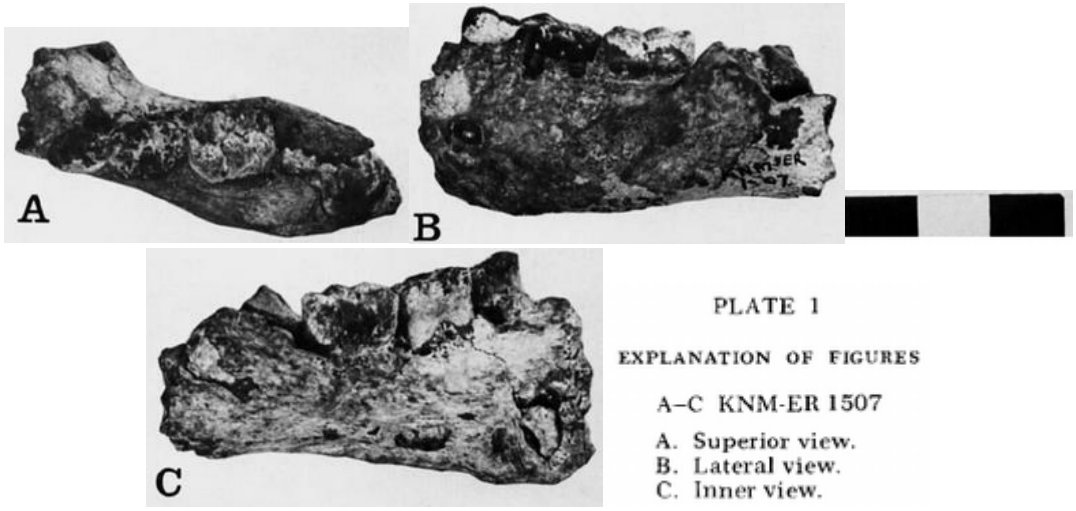

Supplementary Figure S10 – Photograph of the occlusal (A), buccal (B), and lingual (C) aspects of early *Homo* KNM-ER 1507 (After Plate 1 in Leakey and Wood, 1974[12]). See Fig. 5 in Dean, 1987[9] for a radiograph of the developing teeth of the specimen.

KNM-ER 1507 and 820 have their M_2 and premolars developping at the same pace, although KNM-ER 820 has a slightly more advanced M_2. Dean (1987)[9] also highlight that both early *Homo* are developmentally similar to four *Paranthropus* specimens which are OH30, KNM-ER 1477 (Suppl. Fig. S3), KNM-ER 812 (Suppl. Fig. S4), and KNM-ER 1820 (Suppl. Fig. S5). Yet, Dean (1987) noticed that the early *Homo* infants are both 'dentally more mature than [these] specimens of *P. boisei* described [as] being closer to 5 years of age'[9]. (Words in square brackets are our modifications).

Both early *Homo* specimens are developpementally older than GAR IVE (Suppl. Figs S9 and S10).

1.3. Estimating the age of stress events in the enamel of the LRP4

1.3.1. Time of P4 initiation in early *Homo*

In hominids, both M2 and P4 initiate together ([4,5,7]; see Sts 24 in Suppl. Fig. S8).

Dean and Smith[13] show that the Sangiran S7-37 P^4 and the KNM-WT 15000 M^2 initiate at about the same age, shortly after 2 years. Dean[9] described the stage of development of postcanine teeth in juvenile early *Homo* KNM-ER 820 and KNM-ER 1507 (see Suppl. Figs S9 and S10), and observed that, in each specimen, both premolars seem to parallel their M_2 in terms of developmental stage. Dean [14] further notice that M1 and I1 have coinciding calcification stages in *Paranthropus* and early *Homo* (See Fig. 2.5 in [14]). Interestingly in *Paranthropus robustus*, M2 also initiates shortly after 2 years of age (735 days for ML cusp of SK 62, and 823-888 days for the ML cusp of DNH 108; [7]). To note that *Australopithecus africanus* STS 2 has just fused both cusps in its ULP4 at the time of death at 2.52 years [7]. DNH 35, a South African early *Homo*, has just started the formation of its LRP4 and is at the stage of 3 unfused cusps (See Suppl. Fig. S11). Its age at death was histologically estimated to be 795 days, or 2.18 years [7].

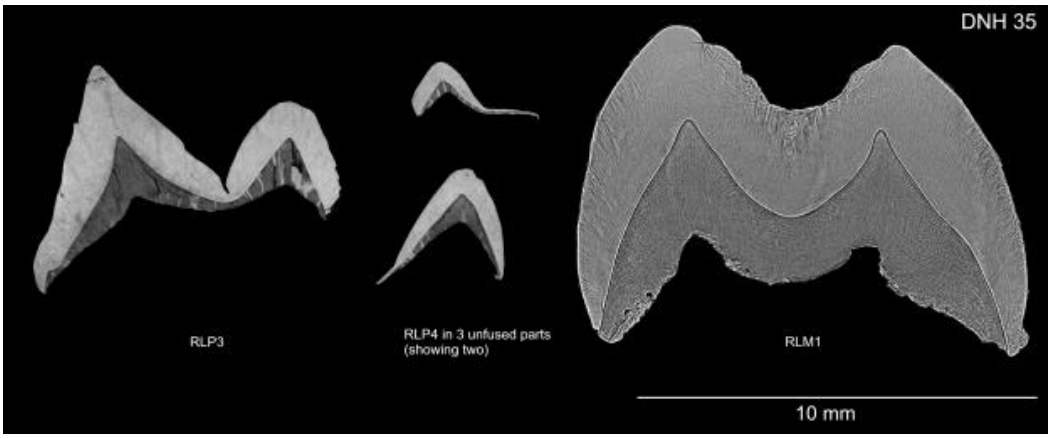

Supplementary Figure S11 –Virtual 2D section through the developmental plane the permanent tooth germs of South African specimen DNH 35 (after Fig. O in S1 file of Smith et al., 2015[7]).

Ramirez Rozzi[15,16] investigated the enamel microstructure of Plio-Pleistocene hominid teeth and concluded that premolars crowns form in 2.54 ± 0.35 years, while molars crowns form in 2.56 ±0.41 years. He further demonstrates that the ratio between the molar and the premolar crown formation times is ~1.01 in Plio-Pleistocene hominids, while it is at 0.77 in modern humans and ranges from 0.6 to 0.75 in great apes [15]. In StW 151, both P4 and M2 seem to reach crown completion at the same time (See Fig. Q in file S1 in [7]). In *Paranthropus robustus* DNH 108, both teeth also seem to have competed their crown at roughly the same time, at ~4.6 years for M^2 (See Fig. N in file S1 in [7]). In DNH 84 (*P. robustus*), the ULP4 has just fused its two cusps and likely completed its cuspal enamel by the time of death at 816 days or 2.2 years (See Fig. L in file S1 in [7]).

In the absence of any histological data for GAR IVE, one can assume an initiation of its LRP4 **shortly after 2 years of age.**

1.3.2. Linear measures stress to dentine horns

On Fig. S1, cuspal enamel thickness in the GAR IVE LRP4 reaches 1363 µm on the lingual cusp and 1 251µm on the buccal cusp. From Fig. Q in Smith et al. [7] (see Suppl. Fig. S12), cuspal thickness can be measured in StW 151: 2388 µm for the lingual cusp, and 2260 µm for the buccal cusp. GAR IVE would thus have just completed 55% of its cuspal enamel.

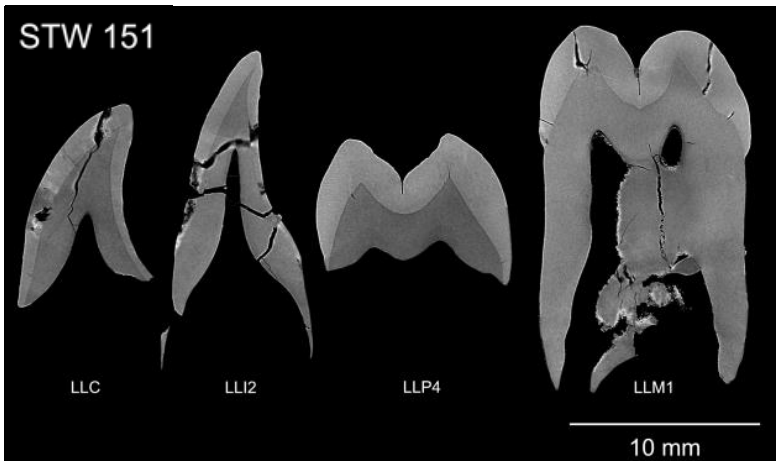

Supplementary Figure S12 –Virtual 2D section through the developmental plane the permanent tooth germs of South African specimen StW 151 (after Fig. Q in S1 file of Smith et al., 2015[7]).

Four accentuated lines (S1 to S4) were identified in the cuspal enamel of the LRP4. In spite of thorough attempts to optimize their visibility by tuning rotation in x,y,z and slice thickness, these accentuated lines could not be identified on a slice passing through the true dentine horn tip. Instead, the virtual thick slice passes through an EDJ ridge (Suppl. Fig. S13). The distance of these lines from the EDJ crest was measured. Keeping in mind the assumed achieved cuspal thickness observed in StW151, S1 to S3 would be in the inner cuspal enamel, while the remainder (including S4) would belong to the middle cuspal enamel.

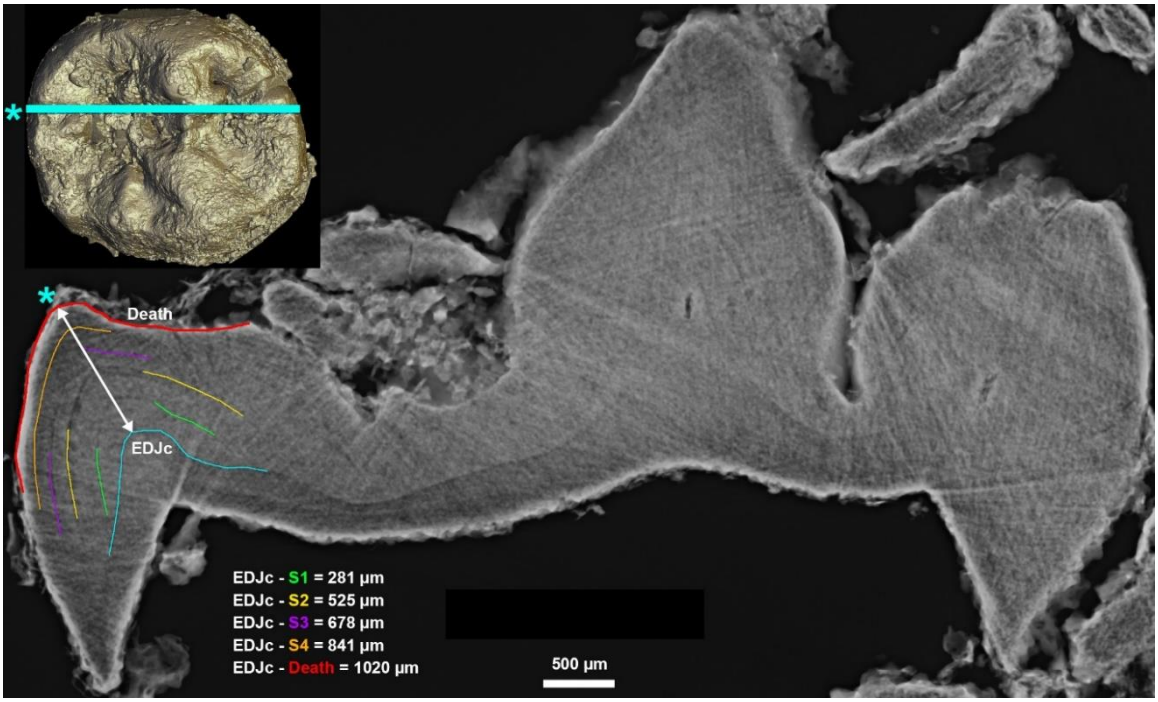

Supplementary Figure S13 – Virtual section (200 µm thick) though the lingual cusp of the GAR IVE LRP4. The orientation of the 2D slice is shown as a blue line on the 3D model. The cusp of interest is marked by an asterisk. Four accentuated lines (S1 to S4) were identified in the cuspal enamel, and their distance to the EDJ crest (EDJc) was measured.

1.3.3. Time of formation of the 4 accentuated lines

Abbreviations used to the following sections:

EDJc: EDJ crest.

S1, S2…, S4: Linear distance in µm between the EDJc and each stress event.

a) Published regression equation for enamel formation time in early *Homo*

Dean et al.[17] have published lowess regression equations for enamel formation rates in hominins. They especially report an equation based on six early *Homo* specimens:

$$y = 3.76 + 0.26x - 0.00002x^2, (R^2 = 0.99, \text{s.e.} = 0.01, P < 0.0001)$$

Based on the linear distances measured in 1.3.2., this equation yields the following times of formation:

Lingual cusp	Distance (µm)	Time (day)	Time (month)	Time between stress events (months)
EDJc	0			
S1	281	75.2	2.51	
S2	525	134.7	4.49	2.0
S3	678	170.8	5.69	1.2
S4	841	208.3	6.94	1.2
Death	1020	248.2	8.27	1.3

Supplementary Table S4 – Distances from the accentuated markings to the EDJ crest of the lingual cusp of GAR IVE LRP4, and corresponding formation time using Dean et al.[17]'s regression formula.

The stress events occur on average every ~1.4 months (Suppl. Table S4), whatever their cause (e.g., illness, food deficiencies).

b) Published enamel daily secretion rates (DSR) for early *Homo*

In their appendix 1, Lacruz et al. [18] published enamel daily secretion rates (DSR) for two African early *Homo* specimens. Because the stress in the GAR IVE LRP4 are located in the cuspal enamel, we consider only their cuspal DSR (Suppl. Table S5).

				Cuspal DSR				
Taxon	Tooth	Specimen	**Cu.out**	**Cu.mid**	**Cu.inn**		**Average per specimen**	**Overall average**
H. habilis	PM	KNM-ER 1805	5.21	4.6	3.68		**4.50**	
H. erectus	PM	KNM-ER 3733	5.28	4.54	4		**4.61**	**4.55**
Average per anatomical region			**5.25**	**4.57**	**3.84**			
		Overall average		**4.55**				

Supplementary Table S5 – Cuspal daily secretion rates collected from Lacruz et al.[18] (in µm/day), and average values.

Applying their average cuspal DSR rate of 4.55 µm/day to the linear distances of each stress to the EDJ crest tip yields the associated formation time (Suppl. Table S6).

Lingual cusp		mean Cu.DSR =	4.55	µm/d
	Distance (µm)	**Time (days)**		
EDJc	0			
S1	281	61.8		
S2	525	115.4		
S3	678	149.0		
S4	841	184.8		
Death	1020	224.2		

Supplementary Table S6 – Formation times of the accentuated marking identified in the GAR IVE LRP4 calculated using the average cuspal DSR (data from Lacruz et al.[18], see Suppl. Table S5).

Considering that S1 to S3 are in the inner cuspal enamel, and S4 to death in the middle cuspal enamel, one can apply the local rates provided by Lacruz et al.[18] (Suppl. Table S7).

Lingual cusp		**Distance (µm)**	**Time (days)**
	EDJc	0	
Inner cuspal	**S1**	281	73.2
DSR = 3.84 µm/day	**S2**	525	136.7
	S3	678	176.6
Middle cuspal	**S4**	841	184.0
DSR = 4.57 µm/d	**Death**	1020	223.2

Supplementary Table S7 – Formation times of the accentuated marking identified in the GAR IVE LRP4 calculated using local cuspal DSR from Lacruz et al.[18], and reported in Suppl. Table S5.

c) Cross-validation and comparison of the two approaches

The overall mean difference between formation times calculated using Dean et al.[17]'s equation and Lacruz et al.[18]'s average cuspal DSR remains acceptable, at ~20 days (Suppl. Table S8). The difference gets even smaller when using the local rates ~9 days, the best result being when using inner cuspal enamel DSR.

	Time of formation for the 4 stress events (in days)				
	Dean et al. (2001)	Lacruz et al. (2008) *average* CuDSR	Difference	Lacruz et al. (2008) *local* CuDSR	Difference
EDJc					
S1	75.2	61.8	13.5	73.2	2.1
S2	134.7	115.4	19.4	136.7	-2.0
S3	170.8	149.0	21.8	176.6	-5.7
S4	208.3	184.8	23.4	184.0	24.2
Death	248.2	224.2	24.0	223.2	25.0
			20.4		**8.7**
			(= average)		(= average)

Supplementary Table S8 – Cross-validation of the calculation for the formation times of the accentuated marking identified in the GAR IVE LRP4 by comparing values obtained using three different methods (see Suppl. Tables S4, S6, S7).

We choose to further use the times calculated using Dean et al. [17]'s equation.

1.3.4. Age of the five stress events

Assuming the initiation time of P4 (~2 years) and that the EDJ crest where the virtual slice was recorded formed ~3 months after the dentine horn tip, these were added to the *times* of formation of each stress line will yield an *age* of formation (Suppl. Table S9).

Assumed initiation of P4 in early *Homo:* **ca. 2 years + ~0.25 year (EDJ crest)**		
	Dean et al. (2001)	Age of formation of the stress events (years)
EDJc		2.2
S1	75.2	2.5
S2	134.7	2.6
S3	170.8	2.7
S4	208.3	2.8
Death	248.2	2.9

Supplementary Table S9 – Estimation of the age of formation of the accentuated marking observed in GAR IVE LRP4.

When superimposed with the lingual cusp of the GAR IVE LRP4, the most developed cusp of the DNH 35 LRP4 matches with the purple stress "S3" in GAR IVE (see **1.3.2.** and Suppl. Fig. S12), which, following the DNH 35 growth pattern, would have then occurred at ~the 796th day of life of GAR IVE (i.e., 2.18 years). Death occurred~77 days

later in GAR IVE, which correspond to ~873 days or ~2.4 years in the DNH 35 growth pattern. "S3" shows that the calculated estimation is slightly ahead of the developmental stage observed in other early *Homo* specimens (here by 6.5 months at most), yet this is may be accounted for by the variability which is not captured here, and by the uncertainties related to our measurements (e.g., the virtual section does not pass through the dentine horn tip).

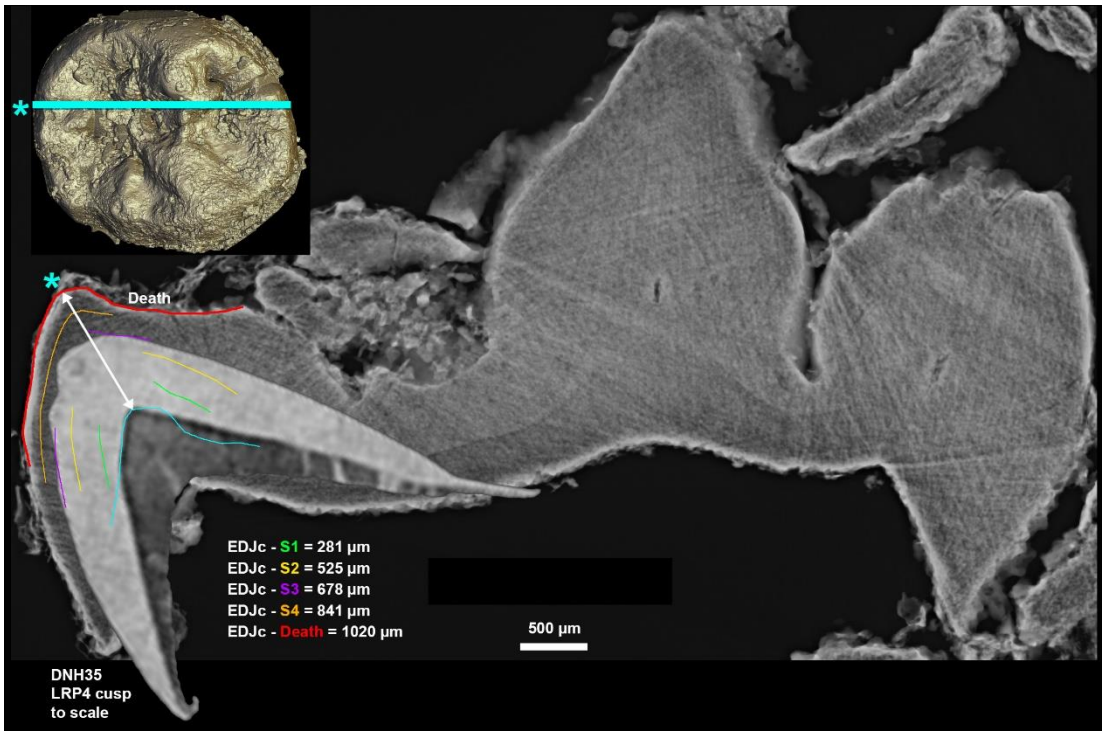

Supplementary Figure S14 – Most developed cusp of the DNH 35 LRP4 (Adapted from Figure O in Smith et al., 2015 [7]) to scale and superimposed to the GAR IVE lingual cusp. The time of death in DNH35 matches the accentuated line S3 in GAR IVE LRP4.

2. Taphonomic investigation of the early Homo *GAR IVE mandible and associated faunal remains. (Suppl. Text S2)*

Surface features

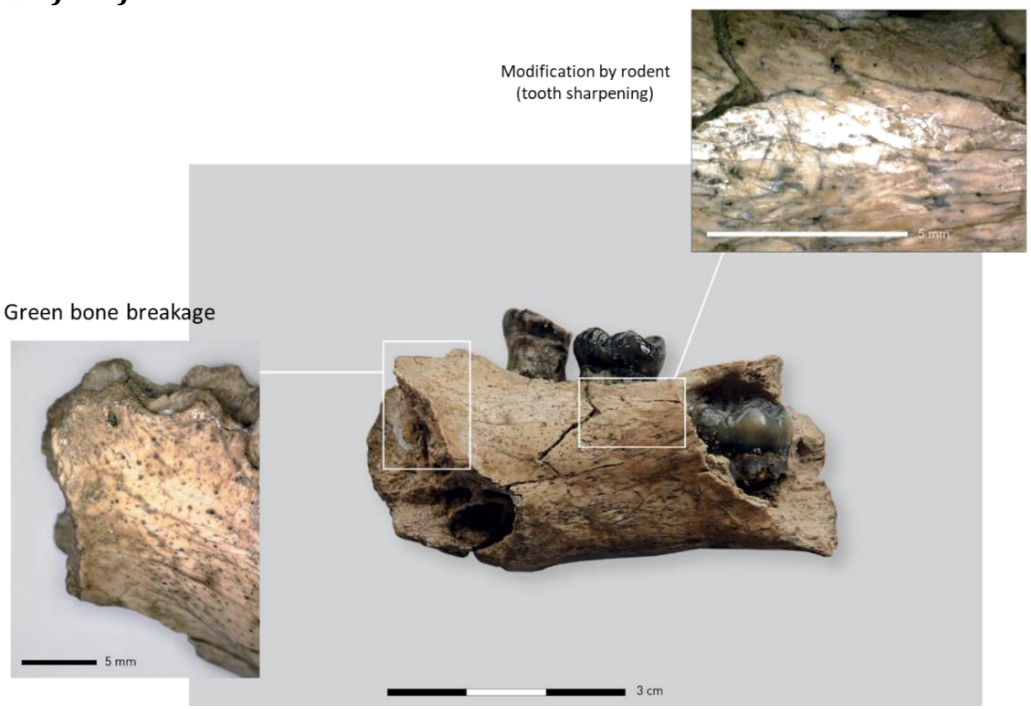

Supplementary Figure S15 – Bone surface modifications on the lingual aspect of the GAR IVE mandible.

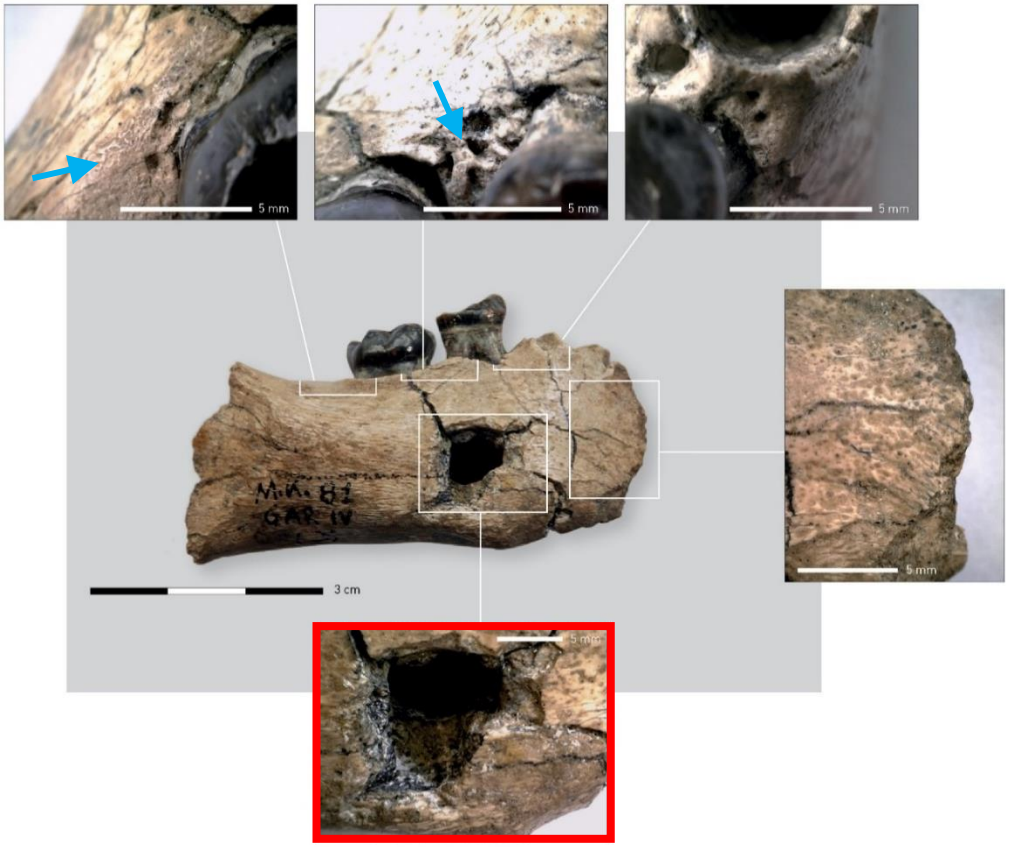

Supplementary Figure S16 – Bone surface modifications on the buccal aspect of the GAR IVE mandible showing the bone perforation in place of the mental foramen (red framed insert), slight weathering on the posterior aspect of the corpus. Note the damages (blue arrows, see Table S12) referred to as „Surface pit,

Class 1" by Parkinson[19], showing striations radiating from the outer circumference of the depression. See also Courtenay et al.[20].

Investigating the role of necrophagous insects in the taphonomic damages observed on GAR IVE.

Dermestids beetles marks on bones represents a particular point in the history of remains, and provides information on the taphonomic processes, including possible season of death[21]. Their occurrence noticeably indicates carcass exposure under warm conditions for several weeks to months and the presence of desiccated tissues during this period[21].

These insects produce various traces, like surface tunnels, pits, and bore holes[19,22]. Such traces have been reported on dinosaur, rhinoceros and *Stegomastodon* bones[22–26], *Bison latifronshorns*[21] and human bones from Bronze Age[27].

Larder beetles (Coleoptera: Dermestidae) are small (0.5 to 1 cm long) necrophagous beetles with a worldwide distribution. Hundreds of species have been reported worldwide, but less than 10 are currently observed on human remains[28]. They are mostly observed on dry corpses, particularly in indoor cases[29,30] or dry outdoor environment[28,31]. On the contrary, dermestid activity does not occur on submerged or buried carcasses[28]. Both larvae and adults are negatively phototrophic and most activity takes place in shaded places.

The larvae feed on dry necrotic tissues, yet bury themselves in a safe place before each molt. After 7 to 8 molts, they stop feeding and dig pupation chambers for nymphosis[32]. These chambers are excavated into adjacent compact surfaces including hard materials such as wood and bone[33]. Two kinds of dermestid traces on bones have been observed: osteophagy and burying of pupation chambers; both can occur at the same time and places[32].

Martin & West[21] defined the following criteria to diagnose dermestid pupation chambers:

(1) The creation of pupation chambers is always associated with presence of carrion.

(2) Pupation chambers on a single bone and necessarily of a given class are uniform in shape and fall within a certain size range (do not vary greatly in size).

(3) Pupation chambers should generally be found in closely associated groups.

(4) Because chambers are usually formed under desiccated tissue that later decays, they are usually found as half casts rather than completely enclosed burrows.

(5) Chambers are excavated by the mandibles and their surface tends to be covered with microscopic depressions representing mandible bites. These

are expressed as small bumps on the casts (these are best studied as casts of the original chamber).

(6) Pupation chambers usually are not much longer than the length of the pupa itself. They are flask shaped with the opening slightly constricted and the main chamber expanded slightly to fit the pupa.

(7) Dermestids, within a species, are fairly uniform in size and the girth of the chamber is a reliable clue for determining if traces found on bone are produced by dermestids.

A close examination of the GAR IVE early *Homo* mandible allows scoring the following features (Suppl. Table S10).

Criteria	**FOR**	**AGAINST**	**Comments**
1	Obvious		
2	Just one chamber, impossible to check		
3		Just one chamber found	Just a small part of the whole skeleton. Pupation chambers were found on faunal remains (see Supplementary Table S12).
4		This chamber looks complete.	Presence of a pre-existing vascular hole (mental foramen).
5		No visible microscopic depressions.	They may have been removed by taphonomic processes or cleaning.
6		The hole is quite deep, not bottle-shaped.	Presence of a pre-existing vascular hole (mental foramen).
7	Internal width of the chamber: 3.4-5 mm		Internal width of the chamber compliant with previous observations (Supplementary Fig. S17), but the outer width is larger than expected (8.02 mm). However, there was a pre-existing vascular hole (mental foramen).

Supplementary Table S10 – Analysis of the Garba IVE early *Homo* mandible according to the 7 criteria defined by Martin & West [21] to diagnose dermestid pupation chambers.

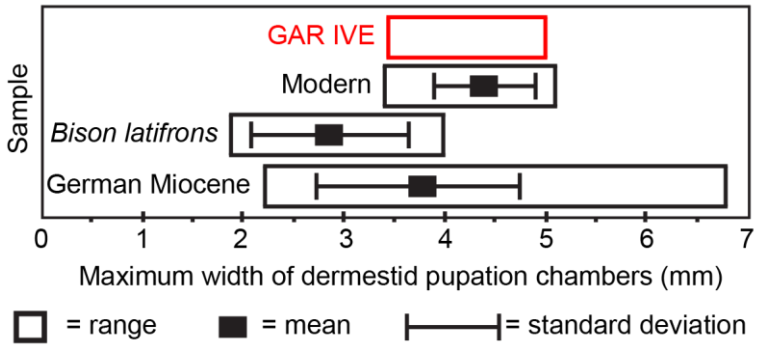

Supplementary Figure S17 – Maximum width of dermestid pupation chambers in modern and palaeontological material, in comparison with the observation made on GAR IVE (modified after Fig. 3 in [21]).

Parkinson[19] also stressed that only the co-occurrence of varying damage types allows for dermestids to be addressed as a variable for bone modification in a fossil faunal assemblage.

Accordingly, and to determine the agent at the origin of the bone perforation seen on the GAR IVE early *Homo* mandible (Figs. 2, 4), a taphonomic study of the associated faunal remains was undertaken. The small sample associated with the early *Homo* mandible originates from layer E and was uncovered during field seasons 2005 and 2009 as well as 1974 and 1975. It was analysed by Fiore and Tagliacozzo[34] (Suppl. Table S11) and is best described as a palimpsest.

However, based on very characteristic damages, 22 specimens can be attributed to the same time-slice within the chain of taphonomic events. Following the nomenclature outlined by Parkinson[19], one can observe surface tunnels (on 9 specimens), bore-holes (on 3 specimens) and surface pits (on 18 specimens). Three specimens showed all three damage-types represented (in red font in Suppl. Table S12).

To note that three specimens show gnawing damage by a small carnivore. Clear indication for bone modification by hominins is not evident.

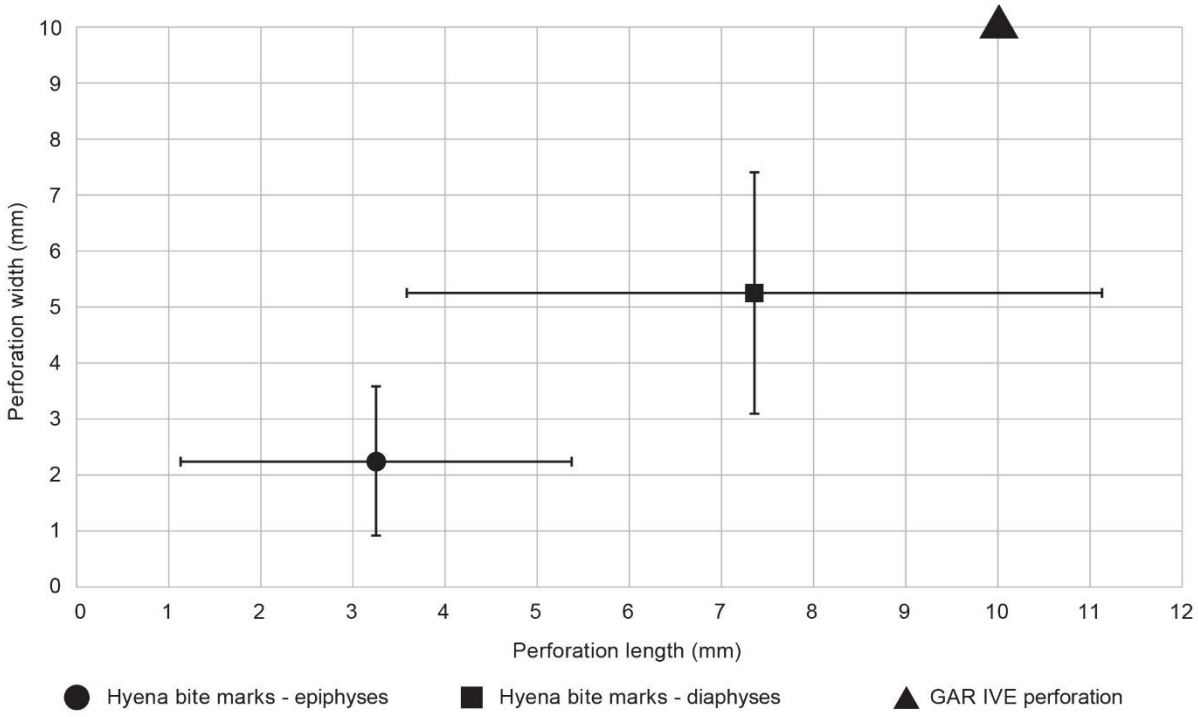

Supplementary Figure S18 – Plot of the size of the Garba IVE perforation on the buccal aspect of its mandibular corpus, in relation to the known dimensions of hyena bite marks on epiphyses and diaphysis as published by Dominguez-Rodrigo and Piqueras[35].

			Sample 2005/2009				Sample 1974/1975 (Fiore & Tagliacozzo 2004)			
Tribe	**Family/Order**	**Genus**	**SC**	**NISP**	**MNI**	**Total 2005/2009**	**NISP**	**MNI**	**Total 1974/75**	**Total sample (n=455)**
Carnivora	Mustelidae	*Enhydriodon aethiopicus*		0		0	1	1	1	**1**
Carnivora				1	1	1	0	0	0	**1**
Equidae	Equus	*Equus* sp.	3	8		8	0	0	0	**8**
Hippopotamidae	Hippopotamus L.	*Hippopotamus* sp.	5	28		28	7		7	**35**
		Hippopotamus cf. *amphibius*	0	0	0	0	1	1	1	**1**
Suidae							1		1	**1**
		Kolpocherus majus	3	1		1	1		1	**2**
Bovidae				11		11	2		2	**13**
	Reduncini	*Kobus* sp.	2	2		2	0	0	0	**2**
	Alcelaphini		4	15		15	1		1	**16**
		Connochaetes sp.	4	5		5				**5**
		Damaliscus sp.	3	0	0	0	1	1	1	**1**
	Antilopini	*Gazella* sp.	2	1		1				**1**
Aves				2	1	2	1		1	**3**
Total tax. det.						74			16	**90**
Indeterminate			1	3		3	2		2	
			2	35		35			0	
			3	23		23	12 *		12	
			4	13		13			0	
			5	11		11	9		9	
			indet.	221		221	7		7	
			not rec.	24		24	5		5	
Total tax. indet.						330			35	**365**

Supplementary Table S11 –Faunal sample composition for Garba IVE.

SC= Size Classes, NISP = Number of identified specimen per taxon, MNI = Minimum Number of Individuals.

*The number of 12 specimens represents large-medium sized (n=5), medium-sized (n=6) and medium-small sized (n=1) taxa [34].

No	Taxon / Size -Class	Fragment	Surface tunnel	Bore hole	Surface pit 1	Surface pit 2	Surface pit 3
05-22	indet. / 4	longbone				x	
05-31	indet. / 3	longbone				x	
05-32	indet. /3	long	x				
05-40	indet. / 3		x	x		x	
05-42	indet. / 2	longbone	x			x	
05-57	indet. / 2	vertebra	x	x			x
05-59	indet. / 3	vertebra					x
05-63	indet. / -	longbone				x	
05-66	indet. / -					x	
05-69	indet. / 3	longbone	x				
05-117	*Hippopotamus sp.* / 5	Mpp				x	
05-364	indet. / 3	longbone	x				x
05-383	*Hippopotamus sp.* / 5	molar				x	
09-1324	indet. / -	longbone	x				
09-1344	indet. / 2	tooth				x	
09-1378	indet. / -						x
09-1604	indet. / -					x	
09-1606	indet. / -	long	x	x		x	
09-1644	indet. / -	long	x				
09-1766	indet. / 3	skull				x	
09-1830	*Hippopotamus* sp. / 5	phalanx				x	

Supplementary Table S12 – Faunal remains with modifications defined by Parkington [19] as diagnostic for dermestid damage. Shaded rows highlight specimens with three types of modifications.

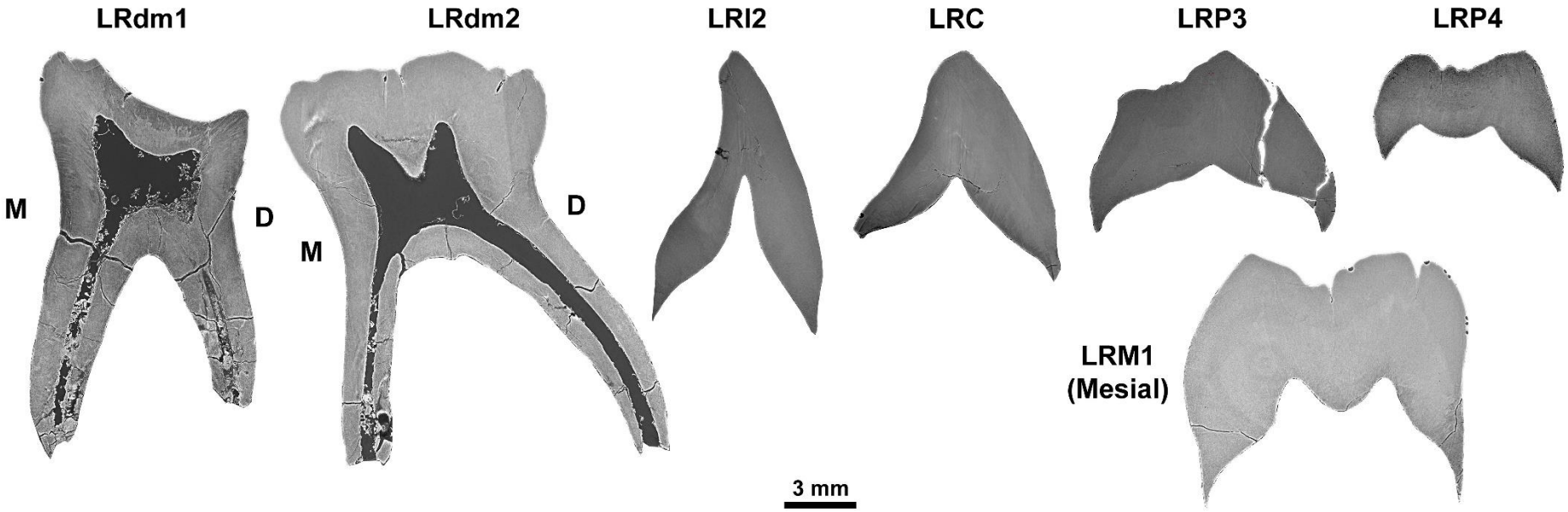

Supplementary Figure S19 –Virtual 2D sections through the GAR IVE teeth showing that there are no significant fractures that could have happened ante-mortem. The teeth are robust and do not look weakened by any pathology. Only a few post-mortem cracks can be seen in the roots of the deciduous molars and on the P3.

3. Reconstruction of the palaeoenvironment. (Suppl. Text S3)

Melka Kunture (8°42'N; 38°35'E) is located 60 km south of Addis Ababa, in a tectonic depression of the Upper Awash Valley of Ethiopia. This is a cluster of paleontological and archaeological sites within a volcanic area active all over the Early and Middle Pleistocene. During Quaternary times, the meandering paleo-Awash River transported and deposited sediments with variable grainsizes. Tephra generated by nearby volcanic eruptions accumulated in the area, clogging up the streams, contributing to the formation of shallow ponds and pools. Ephemeral streams currently erode the Pleistocene deposits and cut gullies, such as the Garba gully, where the site named Garba IV is located, exposing the stratigraphic sequence in natural incisions and allowing identification of archeological deposits which are the focus of excavations. Sedimentological facies suggest a fluvial setting where sedimentation was controlled by the reworking of volcanic material eroded upstream. Fluvial sedimentation of the paleo-Awash alternated with primary volcanic distal fallouts of ashes from the Early Pleistocene Melka series[36].

In Early Pleistocene times, the meandering upper paleo-Awash flowed through a gently undulating landscape[37]. The fluvial channel was slightly further south than the modern river course. The exposed stratigraphic sequence of the Garba IV site starts with silts and sands interbedded with rhyolitic volcanic ash layers and pumice lapilli providing evidence of low-energy fluvial sedimentation in an active volcanic area (Fig. 1c). Mottles suggest periodic backwater. Above, a deposit of pebbles within a sandy matrix (Layer E) is interpreted as the lag deposit of a fluctuating seasonal river. Abundant lithic implements and faunal remains were discovered within this layer. The hominin mandible, which laid on the margin of the river bank, is also part of the record (Fig. 1d). A thin sand deposit capped Layer E and was overlain, in turn, by a primary, partially eroded rhyolitic ash layer, dated at ~1.7 Ma[38].

The fluvial-volcanic context of the Melka area, with its high sedimentation rates provided essential conditions for fast burying of the GAR IVE remains. Acid rains and water could also have affected fossilization processes. In active volcanic regions, ash falls affect both the chemistry of rain and ground waters[39,40]. Waters contaminated by ash leaching are typically enriched in chloride, sulphate and fluoride anions[41]. In modern volcanic settings, ground waters can reach pH as low as 2[42]. In analogy to modern processes, when the late Oldowan layer containing the infant mandible was immersed in a humid environment, it was permeated by water with reduced pH due to leaching through the volcanic ash layers and contamination by volcanic aerosol derived from degassing and eruptions of the volcanoes at short distance from Melka Kunture[40,41].

4. Technical parameters for the µCT data acquisitions. (Suppl. Text S4)

4.1. PPC-SRµCT at the ESRF of GAR IVE.

The GAR IVE mandible was scanned using PPC-SR-µCT on the beamline ID 19 at the ESRF (Grenoble, France). First, an overview scan of the whole specimen was performed at ~25 µm, then the dentition was also scanned at ~6 µm (Suppl. Table S13).

	Overview at ~25 µm	**Overview at ~6 µm**
Date	11/12/2015	12/12/2015
Beamline	ID 19	ID 19
Operator	Dr. Paul Tafforeau	Dr. Paul Tafforeau
Storage ring operating mode (beam delivery)	16 bunch	16 bunch
Energy	100 keV	100 keV
Scintillator	LuAG 2000	LuAG 500
Filters	2.8 mm Al, 6.5 mm Cu	2.8 mm Al, 6.5 mm Cu
Wiggler	W150 gap at 66 mm	W150 gap at 63.2 mm
Phase distance	6400 mm	4400 mm
Synchrotron current	90 mA	70.73 mA
Camera	PCO Edge	PCO Edge
Optic	LAFIP 2	Hasselblad 6 µm
Pixel size	25.37 µm	6.34 µm
Number of projections	2499	8000
Scanning geometry	Normal (No half-acquisition)	Half-acquisition (1000 pixels offset)
Scanning mode	Continuous	Continuous
Number of scans	18	12
Time per scan	2 min 48s (including deadtime of 30s)	7.2 min
Total scanning time	1 h	1 h 40 min
Safety triggering time	1 ms	1 ms
Δz (height per scan)	3.4 mm	5 mm
Exposure time	0.05 s	0.05 s
Darks (no beam)	400 (only once, at the beginning of the acquisition)	100 (at the end)
References (sample out of the beam)	401 (only once, at the beginning of the acquisition)	101 (at the beginning and at the end).
Binning during the acquisition	None	None

Comments	- no contrast at all between dentine and enamel. - ~Homogeneous grey level between bone, enamel and dentine, on both deciduous teeth and permanent tooth germs. - density of enamel ≈ 2.90 - Hypothesis: bone and dentine have been remineralized (taphonomic remodeling). ⇾ Average density in LRC and LRI2 = 3, seems to confirm remineralization.	- still no contrast between enamel and dentine. - EDJ is barely visible from place to place. - No Retzius lines visible. - Perikymata visible in very small areas on few tooth surfaces because of recristallisation occurring on the crowns (i.e., cristals will obliterate the perikymata).

Supplementary Table S13 – Technical parameters for the PPC-SR-µCT acquisition of the overview scans of GAR IVE on the ID 19 beamline at the ESRF.

Each permanent tooth was scanned at ~3.4 µm to image the incremental growth lines (Retzius lines). Last, high-resolution scans were acquired at 0.6 µm in the LRP4 and the LRC, to image the enamel microstructure (Suppl. Table S14).

	Tooth scan at 3.4 µm	High-resolution for enamel microstructure in the LRC and LRP4
Date	13/12/2015	13/12/2015
Beamline	ID 19	ID 19
Operator	Dr. Paul Tafforeau	Dr. Paul Tafforeau
Storage ring operating mode (beam delivery)	16 bunch	16 bunch
Energy	100 keV	~50 keV
Scintillator	LuAG 200	GGG 10
Filters	2.8 mm Al, 5 mm Cu	5.6 mm Al, 0.7 mm Cu, 1 mm diamond
Wiggler	Wiggler W150 gap at 58 mm	Insertion device gap: U176c = 159.9937; W150BT = -0.0314 ; W150B = 259.9931; PPU32A = 11.1012
Phase distance	3400 mm	200 mm
Synchrotron current	77.86 mA	79.9 mA
Camera	PCO Edge	PCO EDGE CAMERALINK (SN 1468)

Optic	Rodenstock	OP-x10-x1 with a lead glass meniscus to protect the optic.
Pixel size	3.41 µm	0.637 µm
Number of projections	8000	8000
Scanning geometry	Half-acquisition (1000 pixels offset)	Half-acquisition (1000 pixels offset)
Scanning mode	Continuous	Continuous
Number of scans	13	1
Time per scan	-	-
Total scanning time	-	-
Safety triggering time	1 ms	5 ms
Δz (height per scan)	5 mm	-
Exposure time	0.1 s	0.1 s
Darks (no beam)	100 (at the end)	100 (at the end)
References (sample out of the beam)	101 (at the beginning and at the end).	101 (at the beginning and at the end).
Binning during the acquisition	None	None
Comments	A few of accentuated lines are visible from place to place mostly in the LRP4, and to a much lesser extent in LRP3 and LRC.	No visible microstructure.

Supplementary Table S14 – Technical parameters for the PPC-SR-µCT acquisition of the middle and high resolution scans of GAR IVE on the ID 19 beamline at the ESRF.

Volumes were reconstructed using a filtered back-projection algorithm (PyHST2 software, ESRF), and Paganin's approach ([43], see [44] for an application at the ESRF). Original 32-bit stacks were converted into 16-bit tiff stacks. The subscans were then concatenated, ring artifact correction was applied as required, and the concatenated subscans were cropped to define the final size (bounding box) of the dataset. Data were saved as JPEG 2000 with a compression factor of 10 (this format minimizes the loss of data quality).

4.2. Conventional µCT at MPI-EVA of the modern comparative samples

(Suppl. Table S15)**.**

	AI_1 (ULM3)	**AI_2**	**AI_3**
Form of AI	rather hypoplastic	?	Maybe hypocalcified
Tooth type	UM3	dm	ULdm2
µCT scanner	diondo d3	diondo d3	diondo d3

Voltage (kV)	120	130	130
Current (µA)	50	40	40
Filters thickness (mm)	0.5 mm Brass	0.5 mm Brass	0.5 mm Brass
Integration time (ms)	1500	1500	1500
Number of projections	2970	2970	2970
Frame average	2	2	2
Pixel size (µm)	5.8618	5.4820	5.4820
Resampled pixel size for segmentation and 3D model (µm)	15	15	15
Scan duration	14h 51min	2h30min	2h30min

Supplementary Table S15 – Technical parameters for the conventional µCT scan acquisitions of the modern human clinical teeth, in the Department of Human Evolution (MPI-EVA, Leipzig, Germany).

Volumes were reconstructed using a filtered back-projection algorithm, beam-hardening and ring artifacts correction were applied as needed. Data were saved as a stack of tiff files. The scans were resampled at 15 µm and filtered using a median and a Kuwahara filter (kernel size of 3 for each; [45]) to facilitate the segmentation in Avizo 6.3.1 (VSG). Enamel thickness was visualized in 3D by computing distances points by point between the enamel and dentine surfaces.

5. Cited references

1. Smith, T. M. *et al.* Dental evidence for ontogenetic differences between modern humans and Neanderthals. *Proc. Natl. Acad. Sci.* **107**, 20923–20928 (2010).
2. Condemi, S. The Garba IV E mandible. in *Studies on the Early Paleolithic site of Melka Kunture, Ethiopia* (eds. Chavaillon, J. & Piperno, M.) 687–701 (2004).
3. Zanolli, C. *et al.* Structural organization and tooth development in a *Homo* aff. *erectus* juvenile mandible from the Early Pleistocene site of Garba IV at Melka Kunture, Ethiopian highlands. *Am. J. Phys. Anthropol.* **162**, 533–549 (2017).
4. AlQahtani, S. J., Hector, M. P. & Liversidge, H. M. Brief communication: the London atlas of human tooth development and eruption. *Am. J. Phys. Anthropol.* **142**, 481–490 (2010).
5. Kuykendall, K. L. Dental development in chimpanzees (*Pan troglodytes*): The timing of tooth calcification stages. *Am. J. Phys. Anthropol.* **99**, 135–157 (1996).
6. Demirjian, A., Goldstein, H. & Tanner, J. M. A new system of dental age assessment. *Hum. Biol.* **45**, 211–227 (1973).
7. Smith, T. M. *et al.* Dental Ontogeny in Pliocene and Early Pleistocene Hominins. *PLoS ONE* **10**, e0118118 (2015).
8. Gunz, P. *et al. Australopithecus afarensis* endocasts suggest ape-like brain organization and prolonged brain growth. *Sci. Adv.* **6**, eaaz4729 (2020).

9. Dean, M. C. The dental developmental status of six East African juvenile fossil hominids. *J. Hum. Evol.* **16**, 197–213 (1987).
10. Leakey, R. E. F. Further Evidence of Lower Pleistocene Hominids from East Rudolf, North Kenya, 1972. *Nature* **242**, 170–173 (1973).
11. Bromage, T. G. & Dean, M. C. Re-evaluation of the age at death of immature fossil hominids. *Nature* **317**, 525–527 (1985).
12. Leakey, R. E. F. & Wood, B. A. New evidence of the genus *Homo* from East Rudolf, Kenya (IV). *Am. J. Phys. Anthropol.* **41**, 237–243 (1974).
13. Dean, M. C. & Smith, B. H. Growth and development of the Nariokotome youth, KNM-WT 15000. in *The First Humans: Origin and Early Evolution of the Genus* Homo (eds. Grine, F. E., Fleagle, J. G. & Leakey, R. E.) 101–120 (2009).
14. Dean, M. C. Growth of teeth and development of the dentition in *Paranthropus*. in *Evolutionary History of the "Robust" Australopithecines* (ed. Grine, F. E.) 43–53 (Aldine de Gruyter Publishing Co., 1988).
15. Ramirez Rozzi, F. V. Enamel growth markers in hominid dentition. *Eur. Microsc. Anal.* 21–23 (1994).
16. Ramirez Rozzi, F. Time of crown formation in Plio-Pleistocene hominid teeth. in *Aspects of Dental Biology: Palaeontology, Anthropology and Evolution* (ed. Moggi-Cecchi, J.) 217–238 (International Institute for the Study of Man, 1995).
17. Dean, C. *et al.* Growth processes in teeth distinguish modern humans from *Homo erectus* and earlier hominins. *Nature* **414**, 628–631 (2001).
18. Lacruz, R. S., Dean, M. C., Ramirez-Rozzi, F. & Bromage, T. G. Megadontia, striae periodicity and patterns of enamel secretion in Plio-Pleistocene fossil hominins. *J. Anat.* **213**, 148–158 (2008).
19. Parkinson, A. H. *Dermestes maculatus* and *Periplaneta americana*: bone modification criteria and establishing their potential as climatic indicators. (Faculty of Science, University of the Witwatersrand, 2012).
20. Courtenay, L. A. *et al.* Obtaining new resolutions in carnivore tooth pit morphological analyses: A methodological update for digital taphonomy. *PLOS ONE* **15**, 1–30 (2020).
21. Martin, L. D. & West, D. L. The recognition and use of dermestid (Insecta, Coleoptera) pupation chambers in paleoecology. *Palaeogeogr. Palaeoclimatol. Palaeoecol.* **113**, 303–310 (1995).
22. Britt, B. B., Scheetz, R. D. & Dangerfield, A. A Suite of Dermestid Beetle Traces on Dinosaur Bone from the Upper Jurassic Morrison Formation, Wyoming, USA. *Ichnos* **15**, 59–71 (2008).
23. Laudet, F. & Antoine, P.-O. Des chambres de pupation de Dermestidae (Insecta : Coleoptera) sur un os de mammifère tertiaire (phosphorites du Quercy) : implications taphonomiques et paléoenvironnementales. *Geobios* **37**, 376–381 (2004).
24. Roberts, E. M., Rogers, R. R. & Foreman, B. Z. Continental insect borings in dinosaur bone: examples from the Late Cretaceous of Madagascar and Utah. *J. Paleontol.* **81**, 201–208 (2007).
25. Bader, K. S., Hasiotis, S. T. & Martin, L. D. Application of forensic science techniques to trace fossils on dinosaur bones from a quarry in the Upper Jurassic Morrison Formation, northeastern Wyoming. *Palaios* **24**, 140–158 (2009).
26. Saneyoshi, M., Watabe, M., Suzuki, S. & Tsogtbaatar, K. Trace fossils on dinosaur bones from Upper Cretaceous eolian deposits in Mongolia: Taphonomic interpretation of

paleoecosystems in ancient desert environments. *Palaeogeogr. Palaeoclimatol. Palaeoecol.* **311**, 38–47 (2011).

27. Huchet, J.-B. *et al.* Identification of dermestid pupal chambers on Southern Levant human bones: inference for reconstruction of Middle Bronze Age mortuary practices. *J. Archaeol. Sci.* **40**, 3793–3803 (2013).
28. Charabidze, D., Colard, T., Vincent, B., Pasquerault, T. & Hedouin, V. Involvement of larder beetles (Coleoptera: Dermestidae) on human cadavers: a review of 81 forensic cases. *Int. J. Legal Med.* **128**, 1021–1030 (2014).
29. Voigt, J. Specific post-mortem changes produced by larder beetles. *J. Forensic Med.* **12**, 76–80 (1965).
30. Schroeder, H., Klotzbach, H., Oesterhelweg, L. & Püschel, K. Larder beetles (Coleoptera, Dermestidae) as an accelerating factor for decomposition of a human corpse. *Forensic Sci. Int.* **127**, 231–236 (2002).
31. Lefebvre, F. & Gaudry, E. Forensic entomology: a new hypothesis for the chronological succession pattern of necrophagous insect on human corpses. *Ann. Société Entomol. Fr. NS* **45**, 377–392 (2009).
32. Sommer, H. G. Cleaning skeletons with dermestid beetles—two refinements in the method. *Curator* **17**, 290–298 (1974).
33. Hinton, H. E. *A Monograph of the Beetles associated with stored Products. Volume I.* vol. I (London, Brit. Mus.(Nat. Hist.), 1945).
34. Fiore, I. & Tagliacozzo, A. Taphonomic analysis of the bone remains from the Oldowan site of Garba IV. in *Studies on the Early Paleolithic site of Melka Kunture, Ethiopia.* (eds. Chavaillon, J. & Piperno, M.) 639–682 (2004).
35. Domínguez-Rodrigo, M. & Piqueras, A. The use of tooth pits to identify carnivore taxa in tooth-marked archaeofaunas and their relevance to reconstruct hominid carcass processing behaviours. *J. Archaeol. Sci.* **30**, 1385–1391 (2003).
36. Kieffer, G., Raynal, J.-P. & Bardin, G. Cadre structural et volcanologique des sites du Paléolithique ancien de Melka Kunture (Awash, Ethiopie): premiers résultats. in *Hommes et Volcans. De l'éruption à l'objet* (eds. Raynal, J.-P., Albore-Livadie, C. & Piperno, M.) 77–92 (2002).
37. Raynal, J.-P. & Kieffer, G. Lithology, dynamism and volcanic successions at Melka Kunture (Upper Awash, Ethiopia). in *Studies on the Early Paleolithic site of Melka Kunture, Ethiopia* (eds. Chavaillon, J. & Piperno, M.) 111–135 (2004).
38. Morgan, L. E. *et al.* A chronological framework for a long and persistent archaeological record: Melka Kunture, Ethiopia. *J. Hum. Evol.* **62**, 104–115 (2012).
39. Harding, D. & Miller, J. M. The influence on rain chemistry of the Hawaiian Volcano Kilauea. *J. Geophys. Res. Oceans* **87**, 1225–1230 (1982).
40. Robock, A. Chapter 53 - Climatic Impacts of Volcanic Eruptions. in *The Encyclopedia of Volcanoes* (ed. Sigurdsson, H.) 935–942 (Academic Press, 2015). doi:10.1016/B978-0-12-385938-9.00053-5.
41. Stewart, C. *et al.* Contamination of water supplies by volcanic ashfall: A literature review and simple impact modelling. *J. Volcanol. Geotherm. Res.* **158**, 296–306 (2006).

42. Cuoco, E. *et al.* Impact of volcanic plume emissions on rain water chemistry during the January 2010 Nyamuragira eruptive event: Implications for essential potable water resources. *J. Hazard. Mater.* **244–245**, 570–581 (2013).
43. Paganin, D., Mayo, S. C., Gureyev, T. E., Miller, P. R. & Wilkins, S. W. Simultaneous phase and amplitude extraction from a single defocused image of a homogeneous object. *J. Microsc.* **206**, 33–40 (2002).
44. Sanchez, S., Ahlberg, P. E., Trinajstic, K. M., Mirone, A. & Tafforeau, P. Three-dimensional synchrotron virtual paleohistology: a new insight into the world of fossil bone microstructures. *Microsc. Microanal.* **18**, 1095–1105 (2012).
45. Wollny, G. *et al.* MIA - A free and open source software for gray scale medical image analysis. *Source Code Biol. Med.* **8**, 20 (2013).